



Viscosity and Interfacial Tension of Binary Mixtures Consisting of Linear, Branched, Cyclic, or Oxygenated Hydrocarbons with Dissolved Gases Using Surface Light Scattering and Equilibrium Molecular Dynamics Simulations

Tobias Klein¹ · Frances D. Lenahan¹ · Ziwen Zhai¹ · Manuel Kerscher¹ · Julius H. Jander¹ · Thomas M. Koller¹ · Michael H. Rausch¹ · Andreas P. Fröba¹

Received: 5 March 2022 / Accepted: 18 March 2022 / Published online: 9 April 2022
© The Author(s) 2022

Abstract

In the present study, the influence of the molecular characteristics of the solvent and solute on the dynamic viscosity and interfacial tension of binary mixtures consisting of a liquid with a dissolved gas is investigated using surface light scattering (SLS) and equilibrium molecular dynamics (EMD) simulations. In detail, binary mixtures consisting of linear, branched, cyclic, or oxygenated hydrocarbons and the solutes hydrogen, helium, methane, water, carbon monoxide, or carbon dioxide are studied in the temperature range between (298 and 573) K and for solute mole fractions up to 0.2. With SLS, the liquid dynamic viscosity and interfacial tension of the binary mixtures could be accessed in macroscopic thermodynamic equilibrium with average expanded uncertainties (coverage factor $k=2$) of (2.4 and 2.3)%, respectively. While EMD simulations were able to predict the influence of the dissolved gases on the interfacial tension of the binary mixtures, the simulations fail to represent the influence of the dissolved gas on the viscosity. Due to the systematic variation of the solvent and solute molecules, the influence of the molecular characteristics, e.g., in the form of size, shape, or polarity, on the thermophysical properties of the mixtures is discussed. Dissolving carbon dioxide, e.g., leads to a reduction of both properties by up to 60% compared to the properties of the pure solvent. Dissolved helium, on the other hand, has only a small influence on the properties of the pure solvent. The influence of dissolved water was found to be negligible in mixtures with an alkane but strongly increases both properties when dissolved in an alcohol, which may be explained by the formation of hydrogen bonds.

Keywords Binary mixtures · Gases · Hydrocarbons · Interfacial tension · Molecular dynamics simulations · Surface light scattering · Viscosity

1 Introduction

In many areas of chemical, biological, and energy engineering, mixtures consisting of liquids with dissolved gases are important working fluids. Processes where the working fluid consists of a liquid with a dissolved gas are, e.g., the synthesis of methanol or dimethyl ether from synthesis gas [1, 2], algae production in photobioreactors [3] as well as waste-water treatment and management [4]. For the efficient design and optimization of such processes, the thermophysical properties of the involved fluid mixtures are required at process-relevant thermodynamic states in terms of temperature T , pressure p , and composition. Here, the viscosity and interfacial tension, which are addressed within this work, are important thermophysical properties characterizing liquids with dissolved gases. The dynamic viscosity η , for example, characterizes the flow field in reactors and pipes and determines the power requirements for pumps and mixers. It is also incorporated in many dimensionless numbers like the Reynolds, Prandtl, or Schmidt number, which are important characteristic numbers for the engineering of apparatuses. In addition, the interfacial tension σ is essential for describing wetting behavior and mass transfer at gas–liquid interfaces and enters into dimensionless numbers like the hydrodynamic Weber or Marangoni number.

Due to the large amount of possible combinations of solvent and solute types, coupled with a wide range of thermodynamic states that is of interest for the different applications, the investigation of η and σ for each thermodynamic state by experiments or computer simulations is not feasible. Therefore, corresponding fluid-property models connecting the property of interest with other thermophysical and/or molecular properties must be developed. For this task, a wide variability of solvent and solute types with different molecular characteristics like weight, size, and polarity must be included in the training sets for their development. Once the models are established, they can be tested for the prediction of the thermophysical properties of systems which have not been included in the development step. For both the development and validation of the models, accurate and reliable experimental data for the thermophysical properties are required.

For the experimental determination of the liquid dynamic viscosity η_L and the interfacial tension σ , the surface light scattering (SLS) technique was used. It probes the dynamics of surface fluctuations at phase boundaries in a contactless manner via the analysis of the temporal behavior of the intensity of the scattered light. Based on a full treatment of the hydrodynamic theory for surface fluctuations [5, 6], viscosity and surface or interfacial tension can be accessed in an absolute way in macroscopic thermodynamic equilibrium without the need for a calibration procedure [7–9]. Until today, SLS investigations have contributed to the accurate determination of viscosity and surface or interfacial tension of various fluid types including reference fluids [7, 9], refrigerants [10–12], ionic liquids [13–16], liquid organic hydrogen carriers [17, 18], and liquids with dissolved gases [19, 20] with typical uncertainties of 2% (coverage factor $k=2$) over a broad range of thermodynamic state.

To complement experimental methods such as light scattering techniques, molecular dynamics (MD) simulations have proven to be a valuable tool in

thermophysical property research [19, 21–26]. MD simulations provide not only the access to multiple thermophysical properties, but they can also be applied to thermodynamic states which can hardly be studied experimentally and allow an insight into the fluid structure on a molecular level. The latter-most advantage is valuable for the identification of structure–property relationships, which can be utilized for the development of prediction models [21, 27, 28]. Equilibrium molecular dynamics (EMD) simulations, which are used in this work, allow the determination of equilibrium and transport properties by analyzing molecular motion under equilibrium conditions [29–31].

The present work represents a continuation of an ongoing research project at the Institute of Advanced Optical Technologies—Thermophysical Properties (AOT-TP) at the Friedrich-Alexander-Universität Erlangen-Nürnberg. This project aims at the characterization of long-chained hydrocarbons, alcohols, and their mixtures with dissolved gases by the determination of viscosity and surface or interfacial tension over a wide range of thermodynamic states via SLS and EMD simulations. In a first step, a temperature-dependent modification of the L-OPLS force field (FF) [32, 33] served for improved predictions of the liquid density ρ_L , η_L , and σ of 12 pure solvents up to $T=573$ K [34]. Based on this modified FF, ρ_L , η_L , and σ of binary liquid mixtures of *n*-hexadecane with *n*-octacosane, 2,2,4,4,6,8,8-heptamethylnonane (HMN), or 1-hexadecanol [35] and, most recently, η_L and σ of binary mixtures consisting of the solvent *n*-hexadecane and the six dissolved gases investigated in this study as well as nitrogen (N_2) were investigated by SLS and EMD simulations between (303 and 573) K [20]. In the present work, η_L and σ of various binary mixtures consisting of a liquid with a dissolved gas are determined using SLS experiments and EMD simulations up to $T=573$ K and mole fractions of the dissolved gas in the liquid phase up to 0.2. As solvents, linear and branched alkanes and alcohols of varying carbon numbers as well as two representatives of cyclic hydrocarbon-based liquid organic hydrogen carriers (LOHCs) are investigated to cover a wide range of molecular size and weight as well as polarity. In detail, 1-hexadecanol, 2-butyl-1-octanol, HMN, 2,6,10,15,19,23-hexamethyltetracosane (squalane), *n*-octacosane, *n*-triacontane, and the LOHC reference system consisting of diphenylmethane (DPM) and its hydrogenated analog dicyclohexylmethane (DCM) are selected. As the solutes, hydrogen (H_2), helium (He), methane (CH_4), water (H_2O), carbon monoxide (CO), and carbon dioxide (CO_2) were chosen for their variety in size, weight, sphericity, and polarity. For binary mixtures of DCM with dissolved CO_2 , where no experimental data for the solubility are given in the literature, measurements using the isochoric-saturation method are performed in addition to the SLS and EMD investigations.

In the following, a brief background on the theory, the experimental procedure, and the data evaluation for the SLS technique is given, followed by information about the density and solubility measurements. Afterward, information relevant for the EMD simulations including the data evaluation are presented. Using the experimental and simulated results for η_L and σ , the influence of the molecular characteristics of the solvent and solute on the thermophysical properties of the mixture is discussed. The influence of the molecular characteristics of the dissolved gas is analyzed by comparing the results for binary mixtures consisting of the six different

gases dissolved in either *n*-octacosane or 1-hexadecanol. Results from our previous publications for η_L and σ of the pure solvents are also used to quantify the influence of the dissolved gas on η_L and σ of the binary mixtures. The influence of the molecular characteristics of the solvent is analyzed by comparing the results for binary mixtures consisting of the solutes He or CO₂ dissolved in various solvents. Because no experimental data for the binary mixtures investigated in this work are currently available in the literature, to the best of our knowledge, a direct comparison with further investigations is not possible.

2 Experimental Section

2.1 Materials and Sample Preparation

The names, sources, purities in mass fraction w or volume fraction φ as specified by suppliers, CAS numbers, and molar masses M of all substances used in this work are provided in Table 1. The procedure for synthesizing DCM is detailed in the Supporting Information of Ref. 18. All solvents were filtered with a polytetrafluoroethylene filter with a pore size of 220 nm to remove particle-like impurities. After filtration, the solvent is then degassed at 313 K at p below 100 Pa for approximately 3 h and stored under an argon atmosphere for further usage. The substances *n*-octacosane and *n*-triacontane are filtered and degassed at approximately 20 K above their respective normal melting point. For each mixture, a fresh sample of approximately 40 mL of the solvent is filled into the cleaned sample cell under ambient conditions. The vapor phase is removed using a vacuum pump before introducing the investigated gas for each system. The systems containing the gases He or H₂ are investigated with constant total p of around (3.5 and 7.0) MPa across the complete T range. With dissolved CH₄, CO, or CO₂, p is varied to maintain a constant mole fraction x of dissolved gas of 0.1 and 0.2, 0.05 and 0.1, and 0.1 and 0.2, respectively. For mixtures containing H₂O, where the mole fraction x of H₂O directly after the sample preparation was approximately 0.04 and 0.08, both components were weighed on a balance with an expanded uncertainty ($k=2$) of 1 mg and added to the sample cell under an argon atmosphere at ambient conditions. The uncertainty of $x_{\text{H}_2\text{O}}$ due to the uncertainty of the balance is $U(x_{\text{H}_2\text{O}})=0.0004$. The composition of each mixture is given in Table 2 together with the results for η_L and σ .

2.2 Isochoric-Saturation Method Combined with Vibrating-Tube Densimetry: Liquid Density and Solubility

Since no data were available for the solubility of CO₂ in DCM, corresponding measurements using the isochoric-saturation method [36] were performed. The experimental setup includes a vibrating-tube densimeter DMA 4200 M from Anton Paar, which was used to determine ρ_L of the binary mixtures. The solubility and ρ_L were measured at p up to 7.1 MPa and T between (323 and 473) K. The results were used to develop a correlation for x_{CO_2} and ρ_L as a function of T and p , which was used to

Table 1 Specifications of the chemical supplier, molar mass M , purification method, and purity of the investigated solvent and solutes

Substance	CAS number	Source	$M/(\text{g}\cdot\text{mol}^{-1})$	Weight fraction w or volume fraction φ purity	Purification method
1-hexadecanol ($\text{C}_{16}\text{H}_{34}\text{O}$)	36653-82-4	Alfa Aesar	242.44	$w = 0.9940^a$	Filtration and evacuation
2-butyl-1-octanol ($\text{C}_{12}\text{H}_{26}\text{O}$)	3913-02-8	Tokyo Chem. Industry	186.33	$w = 0.990^a$	Filtration and evacuation
2,2,4,4,6,8,8-heptamethylnonane ($\text{C}_{16}\text{H}_{34}$)	4390-04-9	ACROS Organics	226.44	$w = 0.980^a$	Filtration and evacuation
2,6,10,15,19,23-hexamethyltetracosane ($\text{C}_{30}\text{H}_{62}$)	111-01-3	Merck KGaA	422.80	$w = 0.989^a$	Filtration and evacuation
<i>n</i> -octacosane ($\text{C}_{28}\text{H}_{58}$)	630-02-4	Alfa Aesar	394.8	$w = 0.9934^a$	Filtration and evacuation
<i>n</i> -triacontane ($\text{C}_{30}\text{H}_{62}$)	638-68-6	Alfa Aesar	422.80	$w = 0.9824^a$	Filtration and evacuation
dicyclohexylmethane ($\text{C}_{13}\text{H}_{24}$)	3178-23-2	self-made	180.33	$w = 0.998^b$	Filtration and evacuation
helium (He)	7440-59-7	Linde AG	4.0026	$\varphi \geq 0.99996^a$	None
carbon dioxide (CO_2)	124-38-9	Linde AG	44.01	$\varphi \geq 0.99995^a$	None
carbon monoxide (CO)	630-08-0	Linde AG	28.01	$\varphi \geq 0.9997^a$	None
methane (CH_4)	74-82-8	Linde AG	16.043	$\varphi \geq 0.999995^a$	None
hydrogen (H_2)	1333-74-0	Linde AG	2.0159	$\varphi \geq 0.999999^a$	None
water (H_2O)	7732-18-5	self-made	18.015	$> 16 \text{ M } \Omega\cdot\text{cm}^c$	Filtration and deionization
argon (Ar)	7440-37-1	Linde AG	39.948	$\varphi \geq 0.99999^a$	None

^aPurity as specified in the certificate of analysis of the supplier^bPurity measured using gas chromatography coupled with mass spectroscopy and flame-ionization spectroscopy^cMeasured specific electric resistance

Table 2 Liquid dynamic viscosity η_L and interfacial tension σ of the binary mixtures of 1-hexadecanol, 2-butyl-1-octanol, HMN, squalane, *n*-octacosane, *n*-triacontane, or DCM with dissolved He, CO₂, CO, CH₄, H₂, or H₂O obtained by SLS under saturation conditions as well as the estimated solute mole fraction in the liquid phase x_{solute} , the liquid density ρ_L , vapor density ρ_V , and the vapor viscosity η_V for each investigated temperature T and pressure p^d

T/K	p/MPa	$100 \cdot x_{\text{solute}}$	$\rho_L/(\text{kg} \cdot \text{m}^{-3})$	$100 \cdot U_r(\rho_L)$	$\rho_V/(\text{kg} \cdot \text{m}^{-3})$	$\eta_V/(\mu\text{Pa} \cdot \text{s})$	$\eta_L/(\text{mPa} \cdot \text{s})$	$100 \cdot U_r(\eta_L)$	$\sigma/(\text{mN} \cdot \text{m}^{-1})$	$100 \cdot U_r(\sigma)$
1-hexadecanol+CO ($x_{\text{CO}} \approx 0.05$)										
348.09	3.076	5.00	800.57	1.0	29.68	19.9	4.905	7.2	25.40	7.5
373.18	3.074	5.01	782.90	1.0	27.66	20.9	2.423	4.0	21.84	3.0
398.12	3.088	5.04	765.00	1.0	25.85	21.9	1.483	2.8	20.05	2.7
423.15	3.062	5.01	746.67	1.0	24.23	22.8	1.001	1.9	18.75	1.6
473.06	3.055	5.02	709.05	1.0	21.60	24.7	0.556	2.2	15.77	1.3
523.08	3.036	5.00	669.93	1.5	20.11	26.6	0.358	2.7	12.55	1.5
572.96	3.078	5.09	629.50	1.5	20.50	28.7	0.247	2.9	9.45	1.8
1-hexadecanol+CO ($x_{\text{CO}} \approx 0.10$)										
348.17	6.143	9.98	800.51	1.0	59.47	20.5	4.788	3.1	22.78	3.3
373.22	6.138	10.00	782.88	1.0	53.99	21.4	2.362	2.4	20.27	1.8
398.15	6.063	9.89	764.98	1.0	50.14	22.3	1.479	2.8	18.65	2.1
423.18	6.094	9.96	746.64	1.0	47.40	23.2	0.980	2.7	17.48	2.6
473.25	6.086	9.99	708.91	1.0	43.68	25.0	0.555	2.1	14.68	1.4
523.12	6.528	10.76	669.90	1.5	40.69	26.8	0.351	2.5	11.62	2.9
573.06	6.071	10.05	629.42	1.5	37.71	28.7	0.241	2.5	8.68	1.6
1-hexadecanol+CH ₄ ($x_{\text{CH}_4} \approx 0.10$)										
348.11	2.505	12.35	800.55	1.0	14.19	12.9	4.398	4.3	22.79	4.7
373.14	2.621	12.24	782.93	1.0	13.80	13.6	2.273	2.0	20.76	2.2
398	2.725	12.18	765.09	1.0	13.37	14.3	1.470	3.2	19.30	3.9
423.11	2.823	12.17	746.70	1.0	12.92	15.0	0.968	4.1	18.07	2.8
473.21	2.903	11.91	708.93	1.0	12.09	16.3	0.542	2.2	15.28	1.7
523.07	3.023	12.13	669.94	1.5	11.89	17.9	0.352	1.9	12.22	1.7
573.16	3.098	12.46	629.34	1.5	13.18	20.2	0.239	2.8	9.14	1.8

Table 2 (continued)

T/K	p/MPa	100·x _{solite}	ρ _L /(kg·m ⁻³)	100·U _r (ρ _L)	ρ _V /(kg·m ⁻³)	η _V (μPa·s)	η _L (mPa·s)	100·U _r (η _L)	σ/(mN·m ⁻¹)	100·U _r (σ)
1-hexadecanol + CH ₄ (x _{CH₄} ≈ 0.20)										
348.17	4.434	21.86	800.51	1.0	25.49	13.2	4.196	2.7	21.77	1.9
373.13	4.728	22.08	782.94	1.0	25.24	13.9	2.128	2.2	19.25	2.1
398.11	5.026	22.46	765.01	1.0	24.91	14.6	1.325	2.2	17.87	1.6
423.08	5.318	22.92	746.72	1.0	24.52	15.3	0.925	1.5	16.70	1.3
473.11	5.738	23.55	709.01	1.0	23.60	16.6	0.516	1.5	13.79	1.1
523.06	6.019	24.15	669.95	1.5	22.93	18.0	0.333	1.8	10.95	1.8
573.06	6.167	24.80	629.42	1.5	23.34	19.8	0.229	2.5	8.02	1.6
1-hexadecanol + H ₂ (x _{H₂} ≈ 0.05)										
347.94	3.496	4.60	800.67	1.0	2.41	10.2	4.978	2.7	25.93	3.6
373.24	3.443	4.60	782.86	1.0	2.24	10.6	2.438	2.5	22.82	2.9
398.21	3.469	4.59	764.93	1.0	2.11	11.0	1.484	1.4	20.87	1.9
423.22	3.453	4.52	746.61	1.0	2.00	11.4	1.017	1.5	19.36	2.0
473.01	3.490	4.62	709.09	1.0	1.93	12.3	0.572	1.5	16.45	1.2
523.07	3.483	4.93	669.94	1.5	2.45	13.1	0.364	2.1	13.18	1.7
572.92	3.520	5.60	629.54	1.5	4.41	13.7	0.251	2.0	9.94	1.5
1-hexadecanol + H ₂ (x _{H₂} ≈ 0.10)										
348.02	6.997	9.22	800.62	1.0	4.71	10.2	4.957	3.2	24.59	2.6
373.15	6.991	9.35	782.93	1.0	4.39	10.6	2.482	2.0	22.46	1.6
398.18	7.003	9.28	764.95	1.0	4.13	11.0	1.530	1.6	20.79	1.8
423.1	6.994	9.16	746.70	1.0	3.91	11.5	1.045	1.7	19.52	1.4
473.28	7.022	9.30	708.88	1.0	3.65	12.4	0.577	2.3	16.32	1.2
523.34	7.007	9.92	669.72	1.5	4.03	13.2	0.364	1.8	13.01	1.7
572.94	7.008	11.16	629.52	1.5	5.84	13.8	0.252	2.8	9.80	1.7

Table 2 (continued)

<i>T/K</i>	<i>p/MPa</i>	100· <i>x_{solute}</i>	$\rho_L / (\text{kg}\cdot\text{m}^{-3})$	100· <i>U_r</i> (ρ_L)	$\rho_V / (\text{kg}\cdot\text{m}^{-3})$	$\eta_V / (\mu\text{Pa}\cdot\text{s})$	$\eta_L / (\text{mPa}\cdot\text{s})$	100· <i>U_t</i> (η_L)	$\sigma / (\text{mN}\cdot\text{m}^{-1})$	100· <i>U_t</i> (σ)	
1-hexadecanol + H ₂ O (<i>x</i> _{H₂O} ≈ 0.04)											
373.13	0.111	4.64	823.57	1.0	0.02	1.3	2.742	2.7	24.84	2.3	
398.13	0.117	4.57	823.64	1.0	0.06	2.5	1.725	2.5	23.97	1.7	
423.13	0.132	4.45	823.02	1.0	0.12	4.2	1.191	1.6	22.75	1.9	
473.11	0.192	4.03	819.96	1.0	0.43	9.2	0.664	1.4	19.48	1.5	
523.15	0.292	3.39	818.18	1.5	1.35	14.4	0.457	1.8	16.58	2.0	
573.15	0.431	2.64	815.16	1.5	3.70	17.2	0.344	2.2	12.86	2.2	
1-hexadecanol + H ₂ O (<i>x</i> _{H₂O} ≈ 0.08)											
373.07	0.124	–	828.49	1.0	0.05	2.4	2.706	4.4	25.10	3.0	
398.25	0.124	8.01	827.35	1.0	0.11	3.9	1.622	1.7	22.97	2.6	
423.22	0.143	7.85	826.35	1.0	0.22	6.3	1.155	2.5	21.90	2.4	
473.18	0.234	7.26	822.58	1.0	0.69	11.8	0.656	3.7	18.68	4.9	
523.22	0.398	6.30	816.86	1.5	1.85	16.5	0.442	1.9	15.53	1.8	
573.23	0.635	5.11	815.39	1.5	4.49	19.5	0.343	2.9	13.08	2.3	
2-butyl-1-octanol + He (<i>p</i> _{He} ≈ 3.5 MPa)											
298.14	3.555	–	830.63	1.0	–	–	19.67	3.5	–	–	
323.15	3.649	–	813.32	1.0	5.44	20.6	6.724	2.2	25.34	5.6	
348.15	3.667	–	795.31	1.0	5.21	21.3	2.674	1.8	22.03	3.3	
373.16	3.740	–	776.57	1.0	4.92	22.3	1.469	2.8	20.13	2.3	
398.17	3.795	–	757.12	1.0	4.69	23.5	0.909	1.9	19.05	1.8	
423.19	3.858	–	736.96	1.0	4.62	24.5	0.620	2.1	17.60	1.5	
473.2	3.912	–	694.51	1.0	5.33	26.0	0.357	2.0	14.03	1.6	
523.21	3.874	–	649.22	1.5	7.60	29.3	0.238	2.6	10.57	1.9	
573.19	3.702	–	601.12	1.5	11.77	20.6	0.170	2.6	7.31	2.1	

Table 2 (continued)

<i>T</i> /K	<i>p</i> /MPa	100· <i>x</i> _{solite}	ρ_L /(kg·m ⁻³)	100· <i>U_r</i> (ρ_L)	ρ_V /(kg·m ⁻³)	η_V (μ Pa·s)	η_L (mPa·s)	100· <i>U_t</i> (η_L)	σ /(mN·m ⁻¹)	100· <i>U_t</i> (σ)
2-butyl-1-octanol + He ($p_{He} \approx 7.0$ MPa)										
298.13	6.975	–	830.63	1.0	–	–	20.95	2.4	27.56	–
323.17	7.047	–	813.30	1.0	10.42	20.5	7.005	3.6	26.60	2.9
348.19	7.176	–	795.28	1.0	9.80	21.5	2.842	2.4	21.93	3.2
373.27	7.222	–	776.48	1.0	9.21	22.5	1.464	3.1	19.98	1.5
398.3	7.284	–	757.02	1.0	8.74	23.4	0.917	2.5	18.75	2.3
423.34	7.314	–	736.83	1.0	8.47	24.3	0.632	2.1	17.44	2.0
473.43	7.415	–	694.31	1.0	8.79	26.2	0.360	2.0	14.01	1.6
523.52	7.358	–	648.93	1.5	10.71	28.3	0.233	2.8	10.51	2.3
573.62	7.156	–	600.69	1.5	14.72	30.6	0.160	3.7	7.02	2.0
2,2,4,4,6,8,8-heptamethylnonane + He ($p_{He} \approx 3.5$ MPa)										
298.19	3.564	–	781.13	1.0	5.80	19.4	3.133	1.7	22.98	3.8
323.14	3.564	–	764.46	1.0	5.40	20.5	1.858	1.2	20.48	3.0
348.17	3.655	–	747.49	1.0	5.10	21.4	1.291	2.3	18.66	2.1
373.17	3.716	–	730.29	1.0	4.85	22.4	0.921	2.5	16.97	2.9
398.15	3.797	–	712.86	1.0	4.63	23.4	0.698	2.8	15.63	2.2
423.17	3.841	–	695.14	1.0	4.41	24.3	0.540	2.7	13.68	2.7
2,2,4,4,6,8,8-heptamethylnonane + He ($p_{He} \approx 7.0$ MPa)										
298.15	7.081	–	781.15	1.0	11.23	19.5	3.423	2.4	23.68	2.4
323.15	7.132	–	764.45	1.0	10.43	20.5	1.965	2.1	20.72	1.5
348.18	7.190	–	747.49	1.0	9.79	21.5	1.347	1.6	19.21	2.9
373.17	7.237	–	730.29	1.0	9.24	22.5	0.977	2.7	17.54	1.3
398.16	7.326	–	712.85	1.0	8.75	23.4	0.729	1.6	15.83	1.7
423.18	7.367	–	695.13	1.0	8.30	24.4	0.552	2.8	13.88	1.3

Table 2 (continued)

<i>T</i> /K	<i>p</i> /MPa	100· <i>x</i> _{solute}	ρ_L /(kg·m ⁻³)	100· <i>U_r</i> (ρ_L)	ρ_V /(kg·m ⁻³)	η_V (μ Pa·s)	η_L (mPa·s)	100· <i>U_t</i> (η_L)	σ /(mN·m ⁻¹)	100· <i>U_t</i> (σ)	
473.3	7.425	–	658.88	1.0	7.45	26.4	0.367	1.6	11.64	2.7	
523.34	7.337	–	621.68	1.5	6.72	28.7	0.252	3.4	8.28	2.5	
573.35	7.129	–	583.50	1.5	6.29	30.6	0.162	8.2	5.38	1.7	
squalane+He (<i>p</i> _{He} ≈ 3.5 MPa)											
298.37	3.522	–	805.80	1.0	–	–	29.19	4.0	–	–	
323.19	3.598	–	789.89	1.0	–	–	10.98	3.2	–	–	
348.15	3.662	–	773.94	1.0	5.15	21.4	5.299	2.7	23.38	2.7	
373.16	3.794	–	758.00	1.0	4.92	22.4	3.090	2.6	22.14	2.9	
398.18	3.828	–	742.09	1.0	4.70	23.3	1.960	2.1	19.84	2.3	
423.21	3.882	–	726.23	1.0	4.48	24.3	1.425	2.5	18.83	1.7	
473.19	3.894	–	694.69	1.0	4.07	26.0	0.870	2.0	16.10	2.5	
523.25	3.894	–	663.28	1.5	3.71	27.8	0.557	2.2	12.65	1.7	
573.26	3.684	–	632.08	1.5	3.57	29.9	0.387	2.3	10.29	1.7	
squalane+He (<i>p</i> _{He} ≈ 7.0 MPa)											
298.14	7.050	–	805.95	0.50	–	–	30.66	2.6	–	–	
323.13	7.123	–	789.93	1.0	–	–	11.38	2.1	–	–	
348.14	7.134	–	773.94	1.0	9.75	21.5	5.629	2.1	23.83	1.7	
373.14	7.236	–	758.01	1.0	9.19	22.5	3.154	1.5	21.60	1.8	
398.13	7.277	–	742.13	1.0	8.70	23.4	2.055	1.4	20.23	2.0	
423.15	7.344	–	726.27	1.0	8.26	24.3	1.470	1.6	18.42	2.3	
473.08	7.415	–	694.76	1.0	7.47	26.1	0.885	1.4	16.18	1.3	
523.05	7.343	–	663.41	1.5	6.83	27.8	0.578	2.8	13.02	2.5	
573.04	7.232	–	632.22	1.5	6.47	29.7	0.395	2.0	10.20	1.8	

Table 2 (continued)

<i>T</i> /K	<i>p</i> /MPa	100· <i>x</i> _{solite}	ρ_L /(kg·m ⁻³)	100· <i>U_r</i> (ρ_L)	ρ_V /(kg·m ⁻³)	η_V (μ Pa·s)	η_L (mPa·s)	100· <i>U_r</i> (η_L)	σ /(mN·m ⁻¹)	100· <i>U_r</i> (σ)
<i>n</i> -octacosane + CO ₂ (<i>x</i> _{CO₂} ≈ 0.12)										
373.27	1.491	12.55	757.80	1.0	23.36	19.0	2.294	2.4	21.17	4.0
398.27	1.739	12.37	741.15	1.0	24.98	20.1	1.665	2.7	19.52	2.2
423.29	1.935	12.06	724.49	1.0	26.30	21.3	1.253	3.2	17.83	2.0
473.28	2.328	12.02	691.20	1.0	27.77	23.4	0.789	1.9	15.21	1.8
523.29	2.578	11.79	657.89	1.5	27.43	25.4	0.533	2.3	12.55	1.9
573.21	2.571	10.92	624.64	1.5	25.23	26.6	0.389	2.6	10.46	2.1
<i>n</i> -octacosane + CO ₂ (<i>x</i> _{CO₂} ≈ 0.22)										
373.14	2.647	22.31	757.89	1.0	41.67	19.3	2.290	2.0	20.67	2.5
398.16	3.131	22.28	741.23	1.0	45.61	20.4	1.630	2.5	19.10	1.9
423.2	3.550	22.14	724.55	1.0	48.30	21.6	1.210	2.6	17.17	2.3
473.19	4.257	21.99	691.26	1.0	50.72	23.7	0.738	1.9	13.76	1.5
523.15	4.737	21.66	657.99	1.5	50.27	25.7	0.520	2.5	11.80	2.4
573.16	4.953	21.04	624.68	1.5	47.84	26.6	0.366	2.2	9.34	2.5
<i>n</i> -octacosane + CO (<i>x</i> _{CO} ≈ 0.05)										
373.16	1.571	5.00	755.05	1.0	14.10	20.7	2.571	2.9	22.04	2.4
398.16	1.619	4.99	739.15	1.0	13.81	21.7	1.783	2.0	20.41	1.4
423.23	1.721	5.15	723.27	1.0	13.44	22.7	1.330	2.3	18.82	2.4
473.14	1.770	4.99	692.17	1.0	12.61	24.5	0.836	1.4	16.21	1.7
523.13	1.864	4.97	661.53	1.5	11.92	26.2	0.568	2.7	13.70	1.7
572.94	1.957	4.95	631.53	1.5	11.67	27.6	0.402	2.6	11.20	1.9
<i>n</i> -octacosane + CO (<i>x</i> _{CO} ≈ 0.10)										
373.2	3.141	10.00	755.03	1.0	28.26	20.9	2.503	3.1	21.39	2.6
398.11	3.258	10.05	739.20	1.0	27.21	21.9	1.778	2.4	19.57	1.5

Table 2 (continued)

<i>T/K</i>	<i>p/MPa</i>	100- <i>x</i> _{solvent}	$\rho_L/(kg\cdot m^{-3})$	100- <i>U_r</i> (ρ_L)	$\rho_V/(kg\cdot m^{-3})$	$\eta_V/(\mu Pa\cdot s)$	$\eta_L/(mPa\cdot s)$	100- <i>U_t</i> (η_L)	$\sigma/(mN\cdot m^{-1})$	100- <i>U_t</i> (σ)	
423.22	3.339	9.99	723.31	1.0	26.33	22.8	1.353	2.3	18.30	2.0	
473.14	3.537	9.98	692.20	1.0	24.95	24.7	0.851	2.1	15.59	2.4	
523.16	3.766	10.05	661.55	1.5	23.86	26.4	0.566	2.7	13.20	1.9	
573.15	3.936	9.96	631.40	1.5	23.04	28.3	0.399	2.6	10.71	1.7	
<i>n</i> -octacosane + CH ₄ (<i>x</i> _{CH₄} ≈ 0.10)											
373.23	1.734	10.09	755.00	1.0	9.07	13.5	2.382	2.4	21.43	2.0	
398.1	1.833	10.12	739.16	1.0	8.95	14.2	1.734	2.0	19.67	2.0	
423.17	1.907	10.11	723.40	1.0	8.75	14.9	1.316	2.2	18.37	2.0	
473.08	1.996	10.11	692.20	1.0	8.16	16.2	0.811	1.8	15.87	1.7	
523.16	1.996	10.07	661.55	1.5	7.40	17.5	0.555	2.2	13.42	2.0	
573.18	1.898	9.93	631.39	1.5	6.65	18.5	0.398	2.3	11.03	1.8	
<i>n</i> -octacosane + CH ₄ (<i>x</i> _{CH₄} ≈ 0.20)											
373.16	3.883	20.12	755.05	1.0	20.60	13.8	2.228	2.1	19.70	2.3	
398.13	4.072	20.20	739.15	1.0	20.04	14.5	1.626	1.8	18.26	2.5	
423.14	4.209	20.21	723.34	1.0	19.39	15.1	1.233	1.6	16.99	1.5	
473.14	4.346	20.17	692.21	1.0	17.84	16.4	0.786	2.1	14.72	1.2	
523.11	4.371	20.36	661.56	1.5	16.08	17.6	0.536	2.2	12.49	1.6	
573.07	4.194	20.37	631.47	1.5	14.32	18.6	0.383	2.0	10.24	1.6	
<i>n</i> -octacosane + H ₂ (<i>p</i> _{H₂} ≈ 3.5 MPa)											
373.25	3.500	9.13	755.00	1.0	2.23	10.6	2.514	2.0	21.82	2.2	
398.13	3.500	8.25	739.14	1.0	2.10	11.0	1.823	2.2	20.43	2.3	
423.19	3.494	7.50	723.30	1.0	1.98	11.4	1.367	2.4	19.03	2.2	
473.17	3.537	6.46	692.16	1.0	1.78	12.3	0.854	1.9	16.59	1.4	
523.16	3.494	5.54	661.52	1.5	1.66	13.3	0.578	1.6	13.98	1.8	

Table 2 (continued)

<i>T/K</i>	<i>p/MPa</i>	100· <i>x</i> _{solute}	$\rho_L/(kg\cdot m^{-3})$	100· <i>U_r</i> (ρ_L)	$\rho_V/(kg\cdot m^{-3})$	$\eta_V/(\mu Pa\cdot s)$	$\eta_L/(mPa\cdot s)$	100· <i>U_t</i> (η_L)	$\sigma/(mN\cdot m^{-1})$	100· <i>U_t</i> (σ)	
573.14	3.488	4.90	631.42	1.5	1.75	15.0	0.406	2.1	11.41	1.6	
<i>n</i> -octacosane + H ₂ (<i>p</i> _{H₂} ≈ 7.0 MPa)											
373.18	6.952	18.13	755.03	1.0	4.39	10.6	2.622	3.5	22.19	1.9	
398.1	7.094	16.71	739.17	1.0	4.13	11.0	1.772	2.3	20.03	2.9	
423.14	6.982	15.00	723.40	1.0	3.90	11.5	1.349	2.1	18.75	1.7	
473.18	6.975	12.73	692.17	1.0	3.49	12.4	0.850	1.3	16.29	1.9	
523.07	6.998	11.11	661.57	1.5	3.20	13.3	0.577	2.4	13.66	1.8	
573.07	6.980	9.80	631.45	1.5	3.18	14.6	0.410	2.4	11.15	1.6	
<i>n</i> -octacosane + H ₂ O (<i>x</i> _{H₂O} ≈ 0.04)											
423.06	0.109	–	724.59	1.0	0.79	23.1	1.340	2.1	19.90	1.3	
473.07	0.157	–	691.29	1.0	0.71	25.1	0.853	2.1	16.72	3.9	
523.08	0.219	–	657.99	1.5	0.64	26.9	0.574	2.9	14.21	2.4	
573.06	0.422	–	624.69	1.5	0.58	28.7	0.404	2.6	11.55	2.7	
<i>n</i> -octacosane + H ₂ O (<i>x</i> _{H₂O} ≈ 0.08)											
423.11	0.127	–	724.61	1.0	0.13	3.85	1.360	2.5	19.76	2.4	
473.1	0.208	–	691.32	1.0	0.23	7.85	0.855	2.5	16.79	2.5	
523.12	0.316	–	658.01	1.5	0.41	11.4	0.592	1.9	14.66	3.1	
573.1	0.716	–	624.72	1.5	1.29	16.3	0.414	1.9	11.49	2.4	
<i>n</i> -triacontane + He (<i>p</i> _{He} ≈ 3.8 MPa)											
373.1	3.714	–	758.53	1.0	4.83	22.4	3.303	1.7	24.06	5.7	
398.15	3.772	–	742.71	1.0	4.62	23.3	2.264	1.8	21.77	2.1	
423.15	3.836	–	727.11	1.0	4.41	24.3	1.540	2.7	19.97	2.8	
473.18	3.887	–	696.42	1.0	4.02	26.0	0.956	2.3	16.77	2.4	
523.17	3.857	–	666.47	1.5	3.64	27.8	0.657	3.5	14.45	2.3	

Table 2 (continued)

<i>T/K</i>	<i>p/MPa</i>	100- <i>x</i> _{solute}	100- <i>U_r</i> (ρ_L)	$\rho_L/(kg\cdot m^{-3})$	100- <i>U_r</i> (ρ_L)	$\rho_V/(kg\cdot m^{-3})$	$\eta_V/(\mu Pa\cdot s)$	$\eta_L/(mPa\cdot s)$	100- <i>U_r</i> (η_L)	$\sigma/(mN\cdot m^{-1})$	100- <i>U_r</i> (σ)
573.18	3.678	–	1.5	637.22	1.5	3.25	29.5	0.469	2.2	12.21	3.1
<i>n</i> -triacontane + He ($p_{He} \approx 7.3$ MPa)											
372.84	7.209	–	1.0	758.70	1.0	9.18	22.4	3.308	3.3	24.09	3.9
397.57	7.310	–	1.0	743.08	1.0	8.52	23.4	2.149	2.5	21.39	1.7
423.05	7.291	–	1.0	727.17	1.0	8.01	24.3	1.655	3.4	20.52	1.6
473.03	7.062	–	1.0	696.51	1.0	7.31	26.1	0.992	4.0	16.96	3.9
523	7.571	–	1.5	666.57	1.5	6.81	27.8	0.669	3.3	14.68	2.7
572.99	7.264	–	1.5	637.33	1.5	6.32	29.5	0.475	2.1	12.05	1.9
<i>n</i> -triacontane + CO ₂ ($x_{CO_2} \approx 0.12$)											
373.09	1.415	11.93	1.0	758.54	1.0	22.30	18.9	2.844	4.3	22.48	4.3
398.08	1.695	12.07	1.0	742.76	1.0	24.44	20.0	1.955	2.7	20.63	3.2
423.07	1.914	11.94	1.0	727.16	1.0	26.09	21.2	1.413	2.4	18.35	1.8
473.06	2.350	12.14	1.0	696.49	1.0	27.86	23.3	0.891	2.1	15.54	1.9
523.04	2.568	11.75	1.5	666.55	1.5	27.46	25.2	0.597	1.9	12.93	1.8
572.99	2.537	10.78	1.5	637.33	1.5	24.71	26.5	0.418	3.3	10.31	2.0
<i>n</i> -triacontane + CO ₂ ($x_{CO_2} \approx 0.22$)											
373.12	2.608	21.98	1.0	758.52	1.0	40.92	19.4	2.582	3.4	20.56	3.0
398.16	3.079	21.91	1.0	742.71	1.0	44.92	20.6	1.781	2.5	18.94	4.4
423.16	3.538	22.07	1.0	727.10	1.0	47.72	21.8	1.323	3.1	17.03	2.9
473.2	4.195	21.67	1.0	696.41	1.0	50.44	24.0	0.829	3.7	14.61	2.8
523.23	4.735	21.65	1.5	666.43	1.5	50.18	26.1	0.564	3.1	11.97	2.6
573.2	4.969	21.11	1.5	637.21	1.5	47.62	27.3	0.412	2.7	9.86	3.2
DCM + CO ₂ ($x_{CO_2} \approx 0.14$)											
298.14	1.244	9.87	0.40	874.47	0.40	25.51	15.5	3.402	1.6	26.92	3.5

Table 2 (continued)

<i>T</i> /K	<i>p</i> /MPa	100· <i>x</i> _{solvent}	$\rho_L/(kg\cdot m^{-3})$	100· <i>U_r</i> (ρ_L)	$\rho_V/(kg\cdot m^{-3})$	$\eta_V/(\mu Pa\cdot s)$	$\eta_L/(mPa\cdot s)$	100· <i>U_r</i> (η_L)	$\sigma/(mN\cdot m^{-1})$	100· <i>U_r</i> (σ)
323.07	1.713	11.44	856.85	0.20	31.98	16.8	1.926	1.9	23.42	2.9
347.93	2.186	12.77	839.02	0.25	37.73	18.1	1.287	1.8	21.56	1.3
372.83	2.685	14.09	820.90	0.20	42.43	19.3	0.928	2.1	19.60	2.1
397.72	3.163	15.20	802.50	0.30	45.85	20.5	0.714	1.4	18.18	1.5
422.63	3.516	15.72	783.81	0.25	47.87	21.6	0.564	1.1	16.28	0.64
472.45	3.915	15.68	746.03	0.25	47.67	23.4	0.380	1.5	13.38	2.0
DCM + CO ₂ (<i>x</i> _{CO₂} ≈ 0.25)										
298.13	2.474	19.62	876.13	0.45	53.42	16.0	2.575	1.2	22.38	4.0
323.11	3.326	22.21	858.54	0.25	66.77	17.5	1.572	2.0	19.99	2.3
348.08	4.216	24.61	840.48	0.30	76.30	18.8	1.093	2.9	18.46	2.1
373.16	5.044	26.43	821.78	0.30	83.47	20.2	0.811	1.4	16.71	1.1
398.1	5.682	27.28	802.65	0.35	87.98	21.6	0.631	0.94	15.31	1.2
423.09	6.521	29.15	783.04	0.35	90.01	22.7	0.490	1.7	13.27	1.2
472.91	7.107	28.55	743.24	0.35	87.66	24.6	0.342	2.0	11.03	1.6

^aDirectly measured values for frequency ω_q and damping Γ at a defined wave vector q of surface fluctuations were combined with reference data for ρ_L , ρ_V , and η_V described in the text to determine η_L and σ by an exact numerical solution of the dispersion relation [5, 6]. The relative expanded uncertainties ($k=2$) for the employed properties are $U_r(\rho_V)=5\%$ and $U_r(\eta_V)=10\%$. For ρ_L , η_L , and σ , the relative expanded uncertainties $U_r(\rho_L)$, $U_r(\eta_L)$, and $U_r(\sigma)$, respectively, are given in the table. $U_r(\rho_L)$ for systems which use ρ_L of the pure solvents in the data evaluation are assigned an estimated uncertainty to account for the unknown impact of the dissolved gas. The relative expanded uncertainty ($k=2$) for pressure is $U_r(p)=0.5\%$ for all investigations. The combined expanded uncertainty ($k=2$) for the temperature $U_c(T)$ for the mixtures containing dissolved CO, CH₄, and H₂ is 0.09 K at 348 K and 0.3 K at 573 K and can be interpolated linearly in between. $U_c(T)$ for all other systems is estimated to be 0.02 K at 298 K and 0.8 K at 573 K and can be interpolated linearly in between.

calculate the input parameters for the SLS experiments as given in Table 2. More detailed information on these measurements, the final results for x_{CO_2} and ρ_L , and their correlations as function of T and p are given in the Supporting Information.

2.3 Surface Light Scattering: Liquid Viscosity and Interfacial Tension

The liquid dynamic viscosity η_L and interfacial tension σ are simultaneously determined in an absolute way at macroscopic thermodynamic equilibrium by surface light scattering (SLS). With this technique, photon correlation spectroscopy is used to analyze the temporal behavior of the light scattered from surface waves which are caused by the thermal motion of molecules. The results for η_L and σ are determined by a full solution of hydrodynamic theory for surface fluctuations at the boundary between a liquid phase (subscript L) and a vapor phase (subscript V) given by the dispersion equation $D(\eta_L, \eta_V, \rho_L, \rho_V, \sigma, \Gamma, \omega_q, q)$. Here, ρ_L , ρ_V , and η_V refer to the liquid density, vapor density, and vapor viscosity, while Γ and ω_q describe the damping and the frequency of the surface wave with a specific modulus of the wave vector q . The reader is referred to the literature [5, 6] as well as to our previous studies [9, 37–41] for a detailed description of the theory and application of this technique. A summary of the details relevant for this work is provided below.

For systems with relatively small viscosities and/or large interfacial tensions, as is the case for most measurements in this work, the probed surface fluctuations showed an oscillatory behavior. In this case, a simultaneous determination of η_L and σ is possible by the measured values for damping and frequency reflecting a damped oscillation of the normalized correlation function (CF) of the intensity of the scattered light. For the mixtures of 2-butyl-1-octanol with He at the lowest temperature $T=298$ K and the mixtures of squalane with dissolved He at the lowest two temperatures $T=(298$ and $323)$ K, the surface fluctuations did not propagate ($\omega_q=0$) and the measured CF is associated with two exponentially decaying modes. By disregarding the short-time range of the measured CF where a faster mode of weaker signal strength is present, the second exponential was analyzed with respect to its damping Γ , which is used to determine in a first-order approximation the ratio of σ to η_L . To get access to η_L , data for σ determined at elevated T , where an oscillatory behavior was observed, are correlated with respect to T using a second-order polynomial function and extrapolated to the lower T , where an overdamped behavior was observed. In this way, values for σ can be calculated and used as a further input parameter within the dispersion relation to calculate η_L .

Mixtures containing the dissolved gases H_2 , CH_4 , and CO were investigated within an experimental SLS setup which contains safety measures for handling toxic and explosive gases. All other mixtures are investigated with the experimental setup detailed in our previous study. For the mixtures containing He, CO_2 , and H_2O , the combined expanded uncertainty ($k=2$) for T accounting for the difference of the two T probes is estimated to be $U(T)=0.02$ K at 298 K and $U(T)=0.8$ K at 573 K and can be interpolated linearly in between. For the mixtures containing dissolved CO , CH_4 , and H_2 , $U(T)$ is 0.09 K at 348 K and 0.3 K at 573 K and can be interpolated linearly in between. For all mixtures, the overall relative uncertainty for the reported

pressure, which includes the pressure stability during a measurement series, is 0.5% ($k=2$). In heterodyne SLS experiments where the light scattered by the vapor–liquid interface is superimposed with frequency-unshifted reference light of distinctly larger intensity, six different external angles of incidence relative to the normal of the interface Θ_E were adjusted between (2.5 and 4.0)° in this work.

2.3.1 Data Evaluation

In addition to q , Γ , and, for an oscillatory behavior, also ω_q of the observed surface fluctuations, the liquid and vapor densities, and the vapor viscosity are required input parameters for solving the dispersion relation in order to determine η_L and σ .

In our previous publication on binary mixtures consisting of n -hexadecane and different dissolved gases [20], the influence of the dissolved gas on ρ_L was investigated considering experimental data for binary mixtures of n -hexadecane with dissolved CO_2 , CH_4 , or He. Here, only a small influence of the dissolved gas on ρ_L relative to ρ_L of pure saturated n -hexadecane was found, with an average absolute relative deviation (AARD) between the densities of (0.57, 0.30, and 0.79)% for the solutes He, CO_2 , and CH_4 , respectively, for T between (298 and 473) K. The relatively small impact of the dissolved gas on ρ_L can be explained by the relatively small molecule size and weight of the solute in comparison to the solvent.

With the exception of the binary mixture consisting of DCM and CO_2 , where experimental values for ρ_L are presented in this work, no experimental data for ρ_L are available for any of the present binary mixtures. Since the solvents investigated in this work have the same or even higher molar mass than n -hexadecane, it is assumed that the influence of the dissolved gas is similar or even smaller for the present binary mixtures. Therefore, the influence of the dissolved gas on ρ_L was neglected and ρ_L data of the pure solvents [34] were used as input for solving the dispersion relation. To account for the error that arises from this assumption, the uncertainty of ρ_L was estimated to be 1% in the T range between (298.15 and 473.15) K and 1.5% for T of (523.15 and 573.15) K where the experimental data for ρ_L are extrapolated. In case that ρ_L becomes available for the mixtures for which the pure-component ρ_L data were used as input for the dispersion equation, the values for η_L and σ reported in this work can be corrected using the expressions $\eta_{L,\text{new}} = \eta_{L,\text{this work}} \cdot \rho_{L,\text{new}} \cdot \rho_{L,\text{this work}}^{-1}$ and $\sigma_{\text{new}} = \sigma_{\text{this work}} \cdot \rho_{L,\text{new}} \cdot \rho_{L,\text{this work}}^{-1}$.

The strategy for calculating vapor phase properties η_V , ρ_V , and vapor phase composition is identical to our previous work [20]. Estimated relative expanded uncertainties ($k=2$) for η_V and ρ_V are assumed to be (10 and 5)%, respectively [42]. The composition of the liquid phase was obtained from experimental solubility data from the literature [43–46]. Where the solubility data do not cover the entire T range up to 573.15 K, linear fits between the solute partial pressure and the mole fraction of dissolved gas were used for the extrapolation to high T . For the mixtures containing CO_2 dissolved in n -triacontane, no solubility data are available in the literature. Here, solubility data for CO_2 dissolved in n -octacosane, which has a similar M compared to n -triacontane, were used to estimate the amount of dissolved CO_2 at the given p . Since no solubility data are available also for the binary mixtures consisting of HMN, n -triacontane, squalane, or 2-butyl-1-octanol with dissolved He, they were

investigated at a constant p of (3.5 and 7.0) MPa. Here, the corresponding concentration of He in the liquid phase can be calculated using the specified T and p given in Table 2, should solubility data become available.

The mixtures containing H_2O were investigated as closed systems, where p was monitored during experiments. Due to a lack of solubility data for the mixtures of H_2O and n -octacosane, liquid and vapor compositions were estimated through an iterative calculation scheme detailed in our previous publication [20].

Reported uncertainties in η_L and σ were calculated via an error propagation scheme [37, 39] considering uncertainties introduced by the measured variables and adopted reference data or predictions. Total expanded relative measurement uncertainties ($k=2$), averaged over all investigated systems and thermodynamic states, were determined to be $U_r(\eta_L)=2.4\%$ and $U_r(\sigma)=2.3\%$.

3 EMD Simulations

EMD simulations give access to multiple thermophysical properties by studying the dynamics of atoms and molecules in simulation boxes with a typical side length of a few nanometers. The accuracy of the calculated properties strongly depends on the inter- and intramolecular interactions, which are described by a force field (FF) via atomistic pair-wise potentials. Using a reasonable FF description, the energies and forces between atoms and molecules can then be calculated for each discretized time step of around 1 fs over a total simulation time in the range of (50 to 300) ns for the investigation of transport properties such as viscosity. These calculations are based on classical Newtonian equations of motion. For a detailed description of the underlying theory of EMD simulations, the reader is referred to the respective literature [29–31].

For modeling the solvent molecules studied in this work, the modified version of the L-OPLS FF [34] was taken. This FF is built on the original L-OPLS FF [32, 33] and was modified to better represent equilibrium and transport properties over a wide T range up to 573.15 K by incorporating a T dependency of the Lennard–Jones (LJ) energy parameters. The successful transferability of the modified FF from pure solvents to related mixtures was shown in our previous publications containing results for η_L and σ of binary liquid mixtures [18, 35] as well as mixtures consisting of n -hexadecane with dissolved gases [20]. The FFs for the solutes were the same as those in our previous publications [20].

3.1 Simulation Procedure and Data Evaluation

For detailed information on the simulation procedure as well as the data evaluation for η_L and σ , the reader is referred to our previous publications [20, 34, 35]. In the following, only the details relevant for the simulations in the present work are summarized.

All simulations presented in this work were performed using the GROMACS [47] software package version 5.1.2. In agreement with the original L-OPLS FF

[32, 33], the simulation time step was set to 2 fs and the bonds between the lighter hydrogen atoms and the heavier carbon or oxygen atoms were constrained using the LINCS [48] algorithm. To initialize the simulation boxes, a number of solvent molecules resulting in approximately 30,000 atoms were placed in a cubic simulation box and periodic boundary conditions were established to mimic the bulk behavior. Afterward, solute molecules were added to match the compositions from the SLS experiments. In the cases of HMN, *n*-triacontane, squalane, or 2-butyl-1-octanol with dissolved He where no solubility data are available, the solubility data from the binary mixture of *n*-hexadecane and He [20] were taken to estimate the amount of He dissolved in the liquid phase. To prevent that a possible phase separation during the simulation run falsifies the results, p in the simulations for the calculation of the viscosity was set to be 0.2 MPa above the corresponding saturation p , i.e., in the slightly compressed liquid phase. The following energy minimization, equilibration with respect to T and p , as well as the calculation of η_L and σ are identical to our previous publication [20].

The simulations were performed at $T=(298.15, 323.15, 348.15, 373.15, 423.15, 473.15, \text{ and } 573.15)$ K, while the starting T was adjusted to the melting point of the solvent. The results for η and σ are the average values from three different, independent simulation runs and are reported, together with the thermodynamic state, in Table S4 in the Supporting Information. The stated uncertainties are the double standard deviations ($k=2$) of the three independent simulation runs.

4 Results and Discussion

The results for η_L and σ for all binary mixtures investigated by SLS experiments, together with the input parameters for solving the dispersion relation and their expanded experimental uncertainties, are summarized in Table 2. To study the concentration dependency of η_L and σ , two different mole fractions of the solute x_{solute} were studied experimentally. Here, the binary mixtures with gases of low solubility, i.e., H_2 and He, were studied at fixed p of about (3.5 and 7.0) MPa, while the more soluble gases CH_4 , CO, and CO_2 were investigated at fixed x_{solute} of the dissolved gas. Here, x_{solute} is 0.1 and 0.2 in the case of CH_4 and CO_2 , while it is 0.05 and 0.1 for CO. This differentiation was necessary due to the limitation of p at high T in our SLS setup. While the real mole fraction of dissolved gas is given in Table 2, an approximate x_{solute} for each mixture is used in the discussion for convenience.

In the following, the results for η_L and σ of the binary mixtures investigated by SLS and EMD simulations are shown and discussed. The data for η_L and σ calculated from EMD simulations, together with their thermodynamic states and statistical uncertainties, are given in Table S4 in the Supporting Information. For a direct comparison between the results from SLS and EMD for the binary mixtures studied within this work, the results from both techniques that were performed at the same thermodynamic state are shown in the form of a parity plot in Fig. 1.

For both η_L and σ , a general overprediction of the results independent of the absolute value, and therefore T , by EMD simulations is found. The average relative deviation of the results from EMD simulations from the results from SLS is (27 and

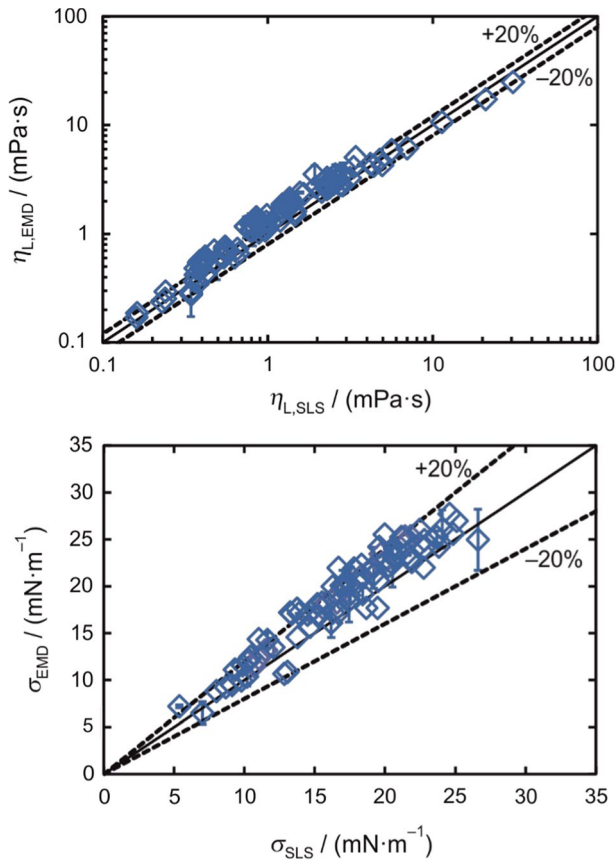


Fig. 1 Comparison of the liquid dynamic viscosity η_L (top) and interfacial tension σ (bottom) of all binary mixtures studied in this work by EMD and SLS. Statistical expanded uncertainties ($k=2$) are shown only exemplarily for the results from EMD simulations

13)% for η_L and σ . This is in agreement with the general overprediction of EMD simulations when applying the modified L-OPLS FF [32–34] found for the pure solvents [34], binary liquid mixtures [35], and mixtures consisting of *n*-hexadecane and different dissolved gases [20, 32–34]. Despite these deviations, it is still possible to investigate the influence of the dissolved gas on both thermophysical properties also by EMD simulations by comparing the results for the binary mixtures to the simulated pure solvent properties. Therefore, for the following discussion of the influence of the molecular characteristics of the solvent and solute molecules on the thermophysical properties of the mixtures, results for the binary mixtures from SLS are compared to the pure solvent properties measured by SLS, while the simulated results for the mixtures are compared to the simulated results of the pure solvent. For the latter, the T -dependent correlations for η_L and σ from EMD simulations are given in the Supporting Information.

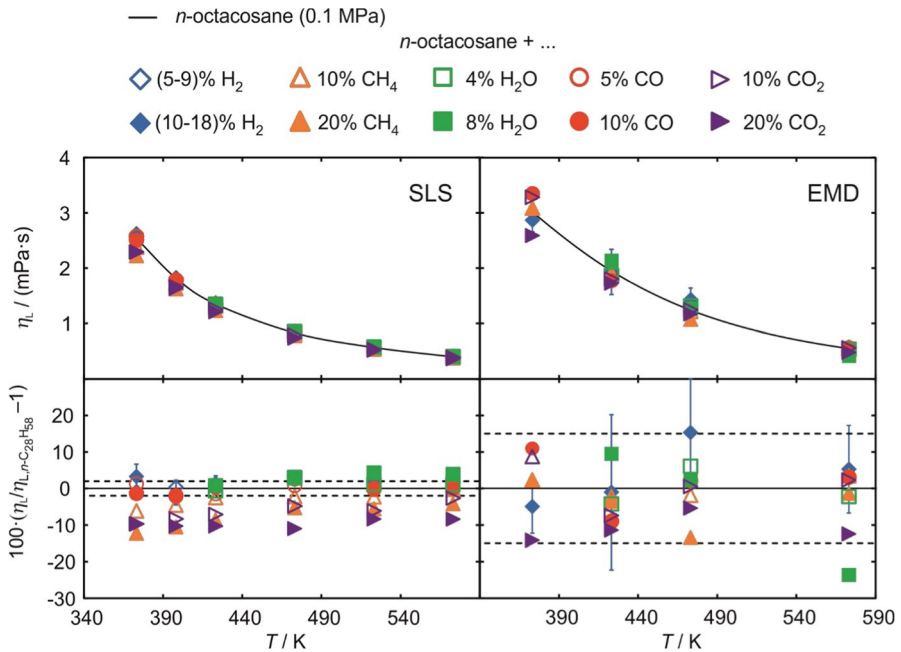


Fig. 2 (Top) Liquid dynamic viscosity η_L of the binary mixtures of *n*-octacosane with the dissolved gases H_2 , CH_4 , H_2O , CO , or CO_2 by SLS (left) and EMD simulations (right) as a function of T and solute mole fraction (open and closed symbols). For comparison, the correlations for η_L of pure *n*-octacosane from SLS [39] and EMD simulations [34] are shown (solid lines). (Bottom) Relative deviations of η_L of the binary mixtures from η_L of pure *n*-octacosane. The dotted lines mark the average expanded uncertainty ($k=2$) of the data for pure *n*-octacosane. Error bars are shown only exemplarily for the mixtures containing H_2 for clarity. The mole fractions of the dissolved gas given in the legend are approximate values. The real composition at each T can be taken from Tables 2 and S4

4.1 Viscosity

The results for η_L for the binary mixtures consisting of *n*-octacosane with dissolved H_2 , CH_4 , H_2O , CO , or CO_2 from SLS experiments (left) and EMD simulations (right) are shown in the upper part of Fig. 2. In addition, the results for η_L of pure *n*-octacosane determined by SLS [39] and EMD simulations [34] and represented by corresponding T -dependent correlations are shown in Fig. 2. As can be seen, the binary mixtures exhibit a similar T -dependent behavior for η_L as the pure solvent. To study the influence of the solute in more detail, the relative deviation of the viscosity of the binary mixtures from that of pure *n*-octacosane is given in the lower part of Fig. 2, which will be discussed in the following.

The binary mixtures containing H_2 , H_2O , and CO show η_L values which agree within combined uncertainties with those of pure *n*-octacosane over the entire T range. For an adequate analysis of this behavior, information about the influence of p on η_L of the pure *n*-octacosane is required. Since no p -dependent data are available for η_L of *n*-octacosane, the influence of p on η_L is estimated with the help of

n-hexadecane. Here, the correlation developed by Meng et al. [49] implemented in the REFPROP database [50] shows an increase in η_L of about (7 and 11)% at $p=(3.5$ and $7.0)$ MPa for $T=298.15$ K. At $T=573$ K, this increase in η_L amounts to (8 and 16)% at $p=(3.5$ and $7.0)$ MPa. This means that the solutes H_2 , H_2O , and CO seem to suppress the p -dependent increase of η_L . The binary mixtures containing CH_4 or CO_2 and studied at elevated p , on the other hand, even have a smaller η_L than pure *n*-octacosane with deviations up to 13%. These results are in qualitative agreement with the investigations for binary mixtures consisting of the same solutes dissolved in further linear alkanes like *n*-hexadecane [20, 51] as well as systems consisting of CO_2 dissolved in *n*-heptane [52] or *n*-tetradecane [53]. A clear difference between the results based on *n*-hexadecane and *n*-octacosane is that the relative deviations are by trend smaller and less dependent on T in the case of *n*-octacosane. This smaller impact of the dissolved gas can be explained with the larger molecule size of *n*-octacosane and, therefore, a stronger entangling at high T where the molecules tend to switch from a *cis*- to *trans*-configuration [21, 27]. This entangling of *n*-octacosane molecules leads to more interstitial space in the fluid structure where the solute molecules can accumulate without hindering the intermolecular interactions between the *n*-octacosane molecules.

The results for η_L from EMD simulations given in the right part of Fig. 2 show that the simulations are not able to resolve the influence of the dissolved gas on η_L considering their uncertainties. Relatively large statistical expanded ($k=2$) uncertainties of η_L of about 15% are typically found in connection with large molecules such as *n*-octacosane, which was already highlighted in the literature [25, 32, 34]. Since the changes in η_L of the binary mixtures relative to the viscosities of pure *n*-octacosane determined by SLS experiments are within 15%, they fall within the expanded statistical uncertainty of the results from EMD simulations.

Next to the rather non-polar *n*-octacosane, also the linear alcohol 1-hexadecanol featuring a polar terminal hydroxyl group was chosen as a solvent to investigate the influence of the solute on η_L and σ of the binary mixtures. For this, binary mixtures consisting of 1-hexadecanol with dissolved H_2 , CH_4 , H_2O , or CO were investigated by SLS and EMD simulations. The results for η_L for these binary mixtures from SLS (left) and EMD simulations (right) are shown in the upper part of Fig. 3. Additionally, the results for η_L of pure 1-hexadecanol investigated by SLS [34] and EMD simulations [34] are shown in Fig. 3. As for the mixtures based on *n*-octacosane, the influence of the solute was examined by calculating the relative deviation of η_L of the binary mixture from that of pure 1-hexadecanol, which is shown in the lower part of Fig. 3.

For the three gases H_2 , CH_4 , and CO dissolved in 1-hexadecanol, the influence of the dissolved gas on η_L determined by SLS is similar as found for the corresponding mixtures based on *n*-octacosane. While the data for mixtures containing H_2 were within combined uncertainties with those for the pure solvent in the case of *n*-octacosane, the difference is more pronounced but still within 5% in comparison with pure 1-hexadecanol at 0.1 MPa. For the solutes CO and CH_4 , a reduction in η_L with maximum deviations of (11 and 19)% from the pure solvent is found, which is similar to the results for mixtures with *n*-hexadecane [20]. In the case of the solute H_2O , however, the binary mixtures show larger values for η_L in comparison to the pure

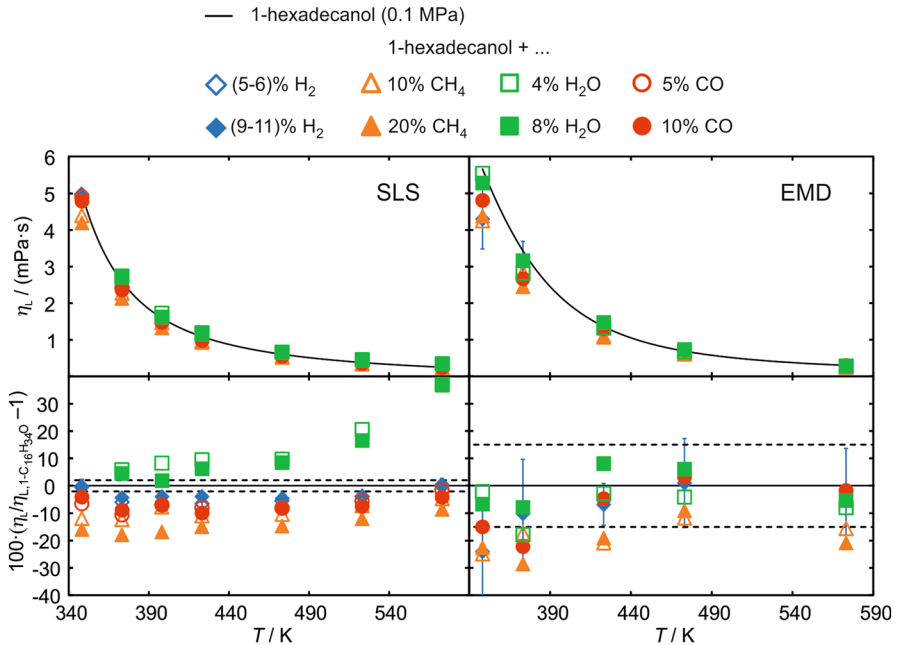


Fig. 3 (Top) Liquid dynamic viscosity η_L of the binary mixtures of 1-hexadecanol with the dissolved gases H₂, CH₄, H₂O, CO, or CO₂ by SLS (left) and EMD simulations (right) as a function of T and solute mole fraction (open and closed symbols). For comparison, the correlations for η_L of pure 1-hexadecanol from SLS [39] and EMD simulations [34] are shown (solid lines). (Bottom) Relative deviations of η_L of the binary mixtures from that of pure 1-hexadecanol. The dotted lines mark the average expanded uncertainty ($k=2$) of the data for pure 1-hexadecanol. Error bars are shown only exemplarily for the mixtures containing H₂ for clarity. The mole fractions of the dissolved gas given in the legend are approximate values. The real composition at each T can be taken from Tables 2 and S4

solvent, while the results for mixtures based on *n*-octacosane or *n*-hexadecane [20] agreed within combined uncertainties with those of the pure solvents at 0.1 MPa. The difference between the data for the mixture and the pure solvent increases strongly with increasing T and reaches a maximum deviation of 37% at the largest investigated T of approximately 573 K. A possible explanation for the much stronger influence of H₂O on η_L of 1-hexadecanol in comparison to the linear alkanes can be found in the formation of hydrogen bonds between the solute and solvent molecules in the bulk of the liquid phase. This agrees with the findings of Ono et al. [54], who showed also an increase of η_L with increasing amount of dissolved H₂O in short primary alcohols especially at high T . An explanation why dissolved H₂O has a much stronger influence at higher T can be found in the work of Lenahan et al. [35]. Here, the authors applied EMD simulations to study the hydrogen bonding between 1-hexadecanol molecules in a binary mixture with *n*-hexadecane as function of T . The results show that strong hydrogen bonds exist between 1-hexadecanol molecules at low T , which vanish with increasing T . The effect of a decreasing amount of hydrogen bonds with increasing T can be explained by the tendency of long molecules

to bend at high T , which hinders the formation of hydrogen bonds due to the steric effect of the alkane tails. With respect to the findings in this work, this means that at low T hydrogen bonds between 1-hexadecanol and H_2O molecules are less likely since the 1-hexadecanol molecules are already forming hydrogen bonds with other 1-hexadecanol molecules. At increasing T , more 1-hexadecanol molecules are available to form hydrogen bonds with H_2O molecules, which leads to an increase in η_L .

The results from EMD simulations, which are shown in the right-hand side of Fig. 3, cannot resolve the influence of the dissolved gas on η_L of the hexadecanol-based mixtures considering the simulated uncertainties. Especially the trend observed by SLS that H_2O causes an increase in η_L of the mixture in comparison to pure 1-hexadecanol is not reflected by the EMD simulations. One possible explanation for this is that the H_2O FF does not consider any T dependency in the FF parameters, which can lead to strong deviations in the predicted properties especially at high T . In the case of the solute CH_4 , the EMD simulations predict an average deviation in η_L from the pure solvent with approximately (18 and 20)% for the mixtures with $x_{\text{solute}}=0.1$ and 0.2 over the entire T range. This agrees with the results from SLS experiments which show a reduction in η_L over the entire T range with an average deviation of (9.3 and 14)% for $x_{\text{solute}}=0.1$ and 0.2.

To study the influence of the molecular characteristics of the solvent on the thermophysical properties of the mixtures, binary systems consisting of either He or CO_2 dissolved in various solvents were investigated by SLS and EMD simulations. The results for η_L for the binary mixtures consisting of He dissolved in HMN, 2-butyl-1-octanol, squalane, or n -triacontane from SLS (left) and EMD simulations (right) are shown in the upper part of Fig. 4. For comparison, also the results for η_L of the pure solvents investigated by SLS [34] and EMD simulations [34] are shown in Fig. 4. To investigate the influence of the solute on η_L for different solvents, the relative deviations of the viscosity of the binary mixtures from that of the pure solvents at 0.1 MPa are given in the lower part of Fig. 4.

The SLS results depicted in Fig. 4 show that the data for η_L of the binary mixtures based on the solvents HMN, squalane, and n -triacontane are mostly within combined uncertainties of the values for the pure solvents. Only for the mixtures investigated at $p=7.0$ MPa, a somewhat larger increase of η_L with respect to the pure solvent of up to 10% can be observed. In the case of the binary mixtures based on 2-butyl-1-octanol, the largest increase is visible for both binary mixtures and amounts up to 14% at $T=298$ K and $p=7.0$ MPa. The stronger influence of dissolved He in 2-butyl-1-octanol on the viscosity in comparison with the other solvents may be attributed to the branched character of the molecule and the effect of p . In comparison to the pure solvent at 0.1 MPa, the increased p present for the mixtures leads to a smaller distance between the molecules, which leads to a stronger entangling due to the side chains in the branched molecules. Because p -dependent data for the η_L of pure 2-butyl-1-octanol are still lacking in the literature, this interpretation cannot be supported. For the branched solvents HMN and squalane, this effect is smaller since they have multiple methyl side chains, which leads to a more compact structure and less entangling.

Also for the EMD simulations, Fig. 4 shows that the results for the binary mixtures are mostly within combined uncertainties of η_L with the pure solvents. The only

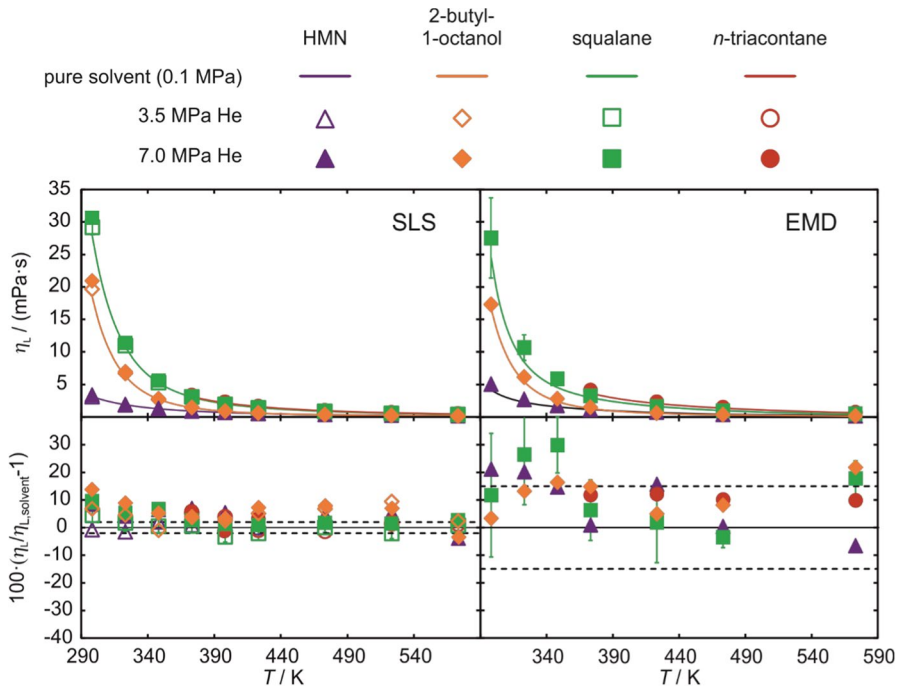


Fig. 4 (Top) Liquid dynamic viscosity η_L of the binary mixtures consisting of He dissolved in HMN, 2-butyl-1-octanol, squalane, or *n*-triacontane investigated by SLS (left) and EMD simulations (right) as a function of T and He pressure (open and closed symbols). For comparison, η_L of the pure solvents investigated by SLS [34] and EMD simulations [34] are shown (solid lines). (Bottom) Relative deviations of η_L of the binary mixtures from η_L of the pure solvents. The dotted lines mark the average expanded uncertainty ($k=2$) of the properties for the pure solvents. Error bars are shown only exemplarily for the mixtures based on squalane for clarity

exception is η_L of the binary mixture based on squalane investigated at $T=348.15$ K, where an approximately 31% larger η_L for the binary mixture in comparison to pure squalane is predicted by the EMD simulations. The results from SLS, on the other hand, show only a difference between the binary mixture and pure squalane of about 10% at this T . As already shown for the binary mixtures based on *n*-octacosane or 1-hexadecanol, this demonstrates that the EMD simulations are not able to quantitatively predict the influence of the dissolved gas on η_L .

To investigate the influence of the solvent characteristics on η_L in connection with a more soluble gas than He, binary mixtures consisting of CO_2 dissolved in the hydrocarbons *n*-octacosane, *n*-triacontane, or DCM were investigated by SLS and EMD simulations. The results for η_L are shown in the upper part of Fig. 5. Additionally, the binary mixtures consisting of DPM with dissolved CO_2 at $x_{\text{CO}_2}=0.1$ or 0.2 were investigated by EMD simulations for $T=(323.15$ to $573.15)$ K. For comparison, also the results for η_L of the pure solvents determined by SLS [17, 34, 39] and EMD simulations [34] are shown in Fig. 5. Relative deviations of η_L of the binary mixture from that of the pure solvents are given in the lower part of Fig. 5.

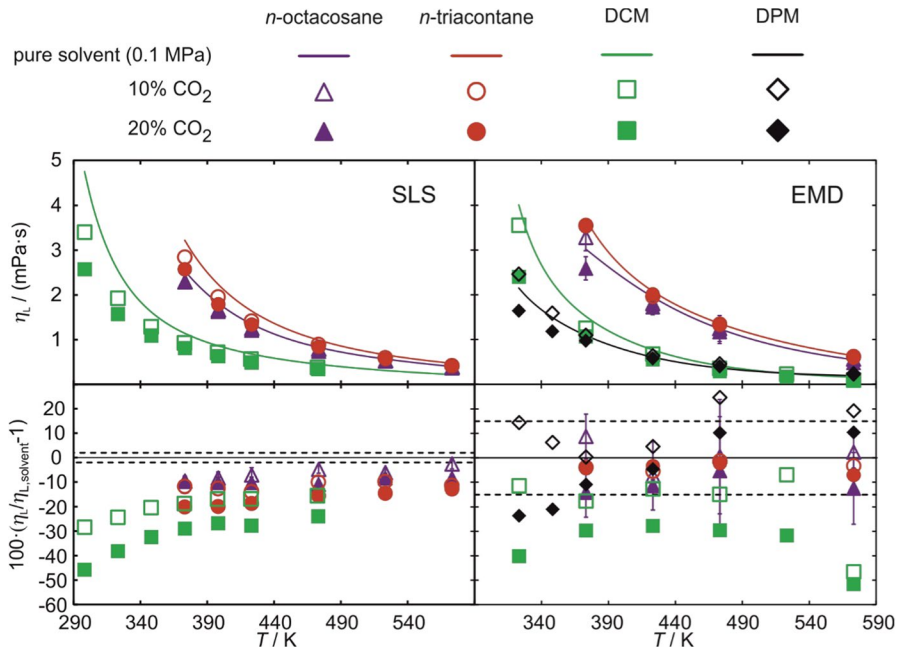


Fig. 5 (Top) Liquid dynamic viscosity η_L of the binary mixtures consisting of CO₂ dissolved in *n*-octacosane, *n*-triacontane, or DCM investigated by SLS (left) and EMD simulations (right) as a function of T and CO₂ mole fraction (open and closed symbols). In the case of EMD simulations, also binary mixtures based on DPM were investigated and are shown. For comparison, the correlations for η_L of the pure solvents based on data obtained by SLS [17, 34, 39] and EMD simulations [34] are shown (solid lines). (Bottom) Relative deviations between the binary mixtures and the pure solvents. The dotted lines mark the average expanded uncertainty ($k=2$) of the viscosity of the pure solvents. Error bars are shown only exemplarily for the mixtures based on *n*-octacosane for clarity. The mole fractions of the dissolved gas given in the legend are approximate values. The real composition at each T can be taken from Tables 2 and S4

The results in Fig. 5 from SLS show a clear reduction in η_L by adding dissolved CO₂ to the three investigated solvents. For the solvent *n*-octacosane, the two binary mixtures show deviations from the pure solvent in the range between -3 and 10% , while the deviation decreases only slightly with increasing x_{CO_2} . In the case of *n*-triacontane, the deviation is larger and ranges between -10 and 20% . For both solvents, the absolute deviation of η_L of the mixture from that of the pure solvents decreases with increasing T . For the binary mixtures based on DCM, the reduction in η_L is more pronounced and ranges up to -46% for the lowest investigated T and $x_{\text{CO}_2}=0.2$. Also in the case of DCM, the deviations decrease with increasing T with approximately -24% at the largest investigated T of 473 K. The general trend of a decrease in the difference between η_L for the binary mixtures and that for the pure solvents, which was also found for mixtures consisting of CO₂ dissolved in *n*-hexadecane [20, 51], can be explained by a decrease in ρ_L with increasing T . This means that at elevated T , the CO₂ molecules can easier occupy the interstitial space in the fluid structure that is created as a result of the decreasing ρ_L . Therefore, the CO₂

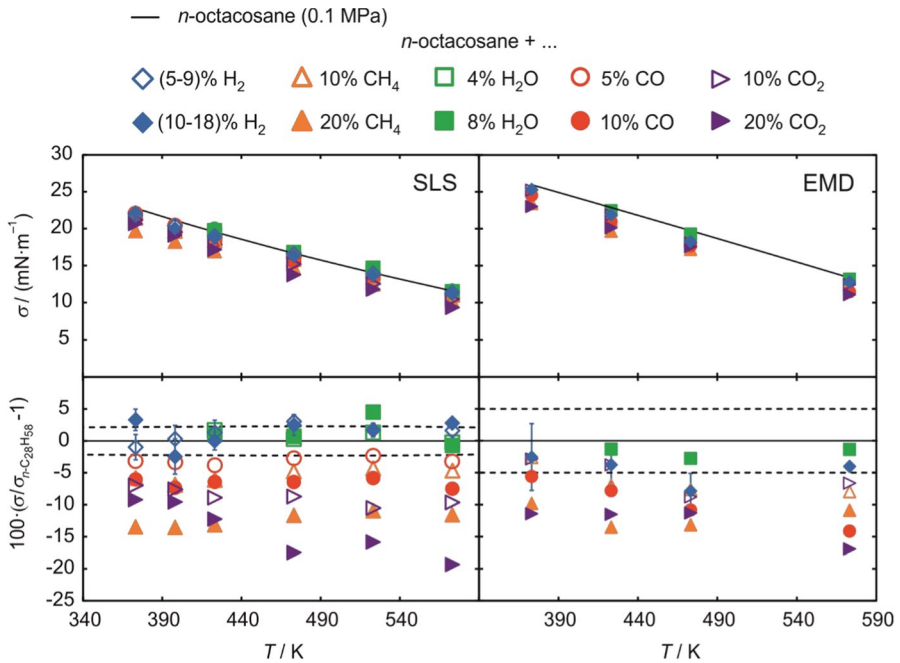


Fig. 6 (Top) Interfacial tension σ of the binary mixtures of *n*-octacosane with the dissolved gases H₂, CH₄, H₂O, CO, or CO₂ by SLS (left) and EMD simulations (right) as a function of T and solute mole fraction (open and closed symbols). For comparison, the correlations for σ of pure *n*-octacosane based on data from SLS [39] and EMD simulations [34] are shown (solid lines). (Bottom) Relative deviations of σ of the binary mixtures from σ of pure *n*-octacosane. The dotted lines mark the average expanded uncertainty ($k=2$) of pure *n*-octacosane. Error bars are shown only exemplarily for the mixtures containing H₂ for clarity. The mole fractions of the dissolved gas given in the legend are approximate values. The real composition at each T can be taken from Tables 2 and S4

molecules seem to disturb the intermolecular interactions between the solvent molecules in a less pronounced way with increasing T .

Also in the case of binary mixtures based on dissolved CO₂, EMD simulations are not able to quantitatively predict the influence of dissolved CO₂ on η_L of the mixtures when compared to the experimental results. The only exception is the binary mixture based on DCM with $x_{\text{CO}_2}=0.2$, where the largest difference between the mixture and the pure solvent is found. Here, EMD simulations predict a reduction in η_L between (40 and 28)% in the range from $T=(323.15$ to $473.15)$ K, which is in good agreement with the observations from SLS.

4.2 Interfacial Tension

Figure 6 shows the results for σ of the binary mixtures consisting of *n*-octacosane with dissolved H₂, CH₄, H₂O, CO, or CO₂ from SLS experiments (left) and EMD simulations (right). In addition, the results for σ of pure *n*-octacosane determined by SLS [39] and EMD simulations [34] represented by a corresponding T -dependent

correlation are shown in Fig. 6. A more detailed resolution of the influence of the solute on σ is provided by the relative deviations of σ of the binary mixture from that of pure *n*-octacosane, which are given in the lower part of Fig. 6 and will be discussed in the following.

In connection with the SLS results for σ shown on the left-hand side of Fig. 6, the results for the binary mixtures containing H_2 and H_2O agree within combined uncertainties with σ of pure *n*-octacosane over the complete T range. For the other solutes, a decrease in σ with increasing amount of dissolved solute with deviations up to -20% can be observed. As it is the case for η_L , the behavior for σ corresponds well with the findings for corresponding binary mixtures based on *n*-hexadecane [20]. Furthermore, in the same way as seen for η_L , the relative deviations of the interfacial tension of the mixtures from that of the pure solvent are smaller for *n*-octacosane than for *n*-hexadecane, especially in connection with CH_4 , CO , and CO_2 . Here, the reader is referred to the interpretation given in the section “Viscosity.”

In the case of σ , which can be determined from EMD simulations with typical statistical uncertainties of 5% [25, 34, 35], the simulations can capture the influence of the dissolved gases. For mixtures based on the solvent *n*-octacosane, the results from EMD simulations show a similar influence of the dissolved gas on σ as found from the experimental investigations. For mixtures based on H_2 and H_2O , for example, EMD simulations show an agreement with σ of pure *n*-octacosane within combined uncertainties over the entire T range investigated. Also for all other solutes, the deviations between the σ data of the binary mixtures and the pure solvent are in good agreement with the findings from SLS experiments.

Next, the influence of the solute characteristics on σ of 1-hexadecanol-based mixtures is discussed using σ data for binary mixtures consisting of 1-hexadecanol with dissolved H_2 , CH_4 , H_2O , or CO . The results for σ for these binary mixtures from SLS (left) and EMD simulations (right) are shown in the upper part of Fig. 7, where also the results for σ of pure 1-hexadecanol obtained from SLS [34] and EMD simulations [34] are included. The influence of the solute was examined by calculating the relative deviation of σ of the binary mixtures from the data for pure 1-hexadecanol, which is depicted in the lower part of Fig. 7.

While σ of mixtures containing H_2 determined by SLS were within combined uncertainties with the data for the pure solvent in the case of *n*-octacosane, the difference is more pronounced but still within 5% with respect to the pure solvent in the case of 1-hexadecanol. For the solutes CO and CH_4 , a reduction in σ with maximum deviations of (15 and 21)%, respectively, is found, which is similar to the results for mixtures with *n*-hexadecane [20]. Similar as seen for η_L , the binary mixtures containing H_2O show larger values for σ in comparison to the pure solvent, while the results for mixtures based on *n*-octacosane or *n*-hexadecane [20] were within combined uncertainties with those of the pure solvents. The difference between the data for the mixture and the pure solvent increases strongly with increasing T and reaches a maximum deviation of 28% at the largest investigated T of approximately 573 K. As already discussed in connection with η_L , a possible explanation for the much stronger influence of H_2O on σ of 1-hexadecanol in comparison to the linear alkanes can be found in the formation of hydrogen bonds

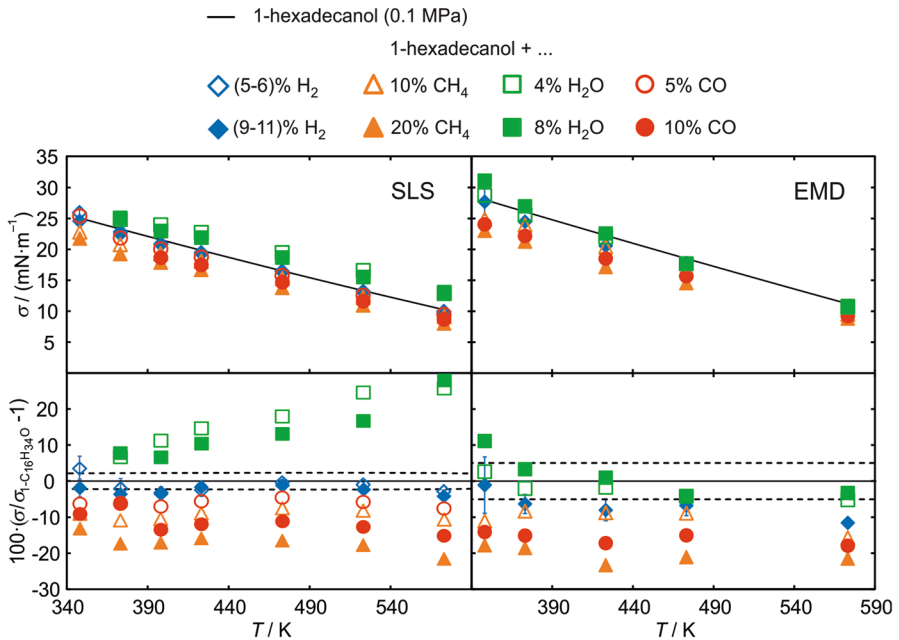


Fig. 7 (Top) Interfacial tension σ of the binary mixtures of 1-hexadecanol with the dissolved gases H_2 , CH_4 , H_2O , CO , or CO_2 by SLS (left) and EMD simulations (right) as a function of T and solute mole fraction (open and closed symbols). For comparison, the correlations for σ of pure 1-hexadecanol based on data from SLS [39] and EMD simulations [34] are shown (solid lines). (Bottom) Relative deviations between the binary mixtures and pure 1-hexadecanol. The dotted lines mark the average expanded uncertainty ($k=2$) of pure 1-hexadecanol. Error bars are shown only exemplarily for the mixtures containing H_2 for clarity. The mole fractions of the dissolved gas given in the legend are approximate values. The real composition at each T can be taken from Tables 2 and S4

between the solute and solvent molecules at the vapor–liquid interface besides that in the liquid bulk phase.

EMD simulations are able to predict the influence of the dissolved gas over the entire T range in the case of the solutes H_2 , CH_4 , and CO . Only for the solute H_2O , the EMD simulations were not able to predict the increase in σ relative to the pure solvent with increasing T , as it was also the case for η_L shown in Fig. 3. This failure in predicting the influence of H_2O on σ and η_L seems to be related to the combination of the modified L-OPLS FF [32–34] for 1-hexadecanol and the SPC/E FF [55] for H_2O , which cannot accurately represent the hydrogen bonding between the solute and solvent molecules, especially at large T .

In the same way as carried out for η_L , the influence of the molecular characteristics of the solvent on σ of the mixtures is studied by investigating binary systems consisting of either He or CO_2 dissolved in various solvents by SLS and EMD simulations. The results for σ for the binary mixtures consisting of He dissolved in HMN, 2-butyl-1-octanol, squalane, or n -triacontane from SLS (left) and EMD simulations (right) are shown in the upper part of Fig. 8. Additionally, the results for σ of pure solvents investigated by SLS [34] and EMD simulations [34]

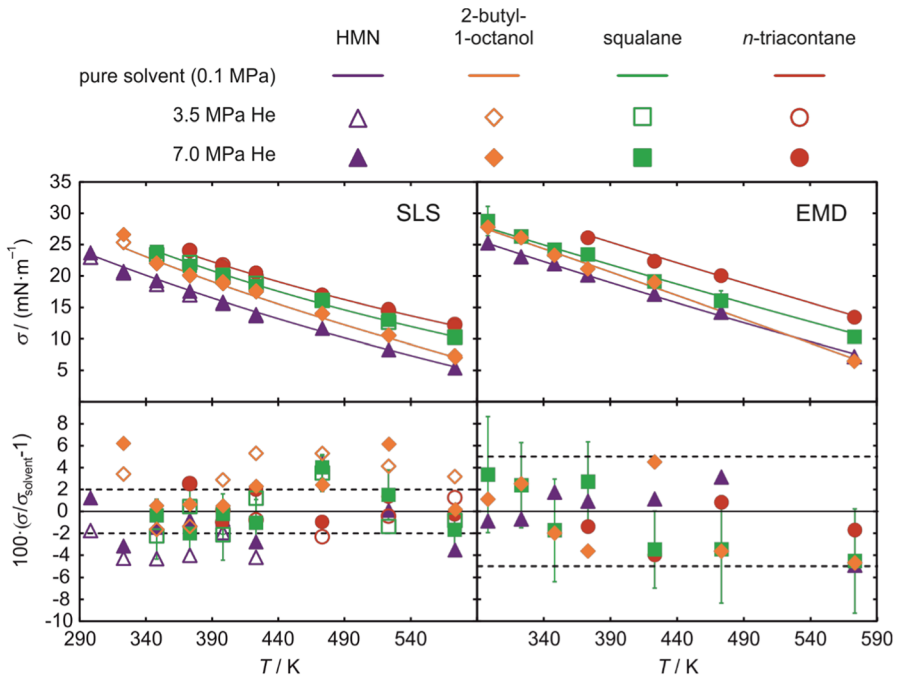


Fig. 8 (Top) Interfacial tension σ of the binary mixtures consisting of He dissolved in HMN, 2-butyl-1-octanol, squalane, or *n*-triacontane investigated by SLS (left) and EMD simulations (right) as a function of T and He mole fraction (open and closed symbols). For comparison, T -dependent correlations σ of the pure solvents investigated by SLS [34] and EMD simulations [34] are shown (solid lines). (Bottom) Relative deviations between σ of the binary mixtures and σ of the pure solvents. The dotted lines mark the average expanded uncertainty ($k=2$) of the properties for the pure solvents. Error bars are shown only exemplarily for the mixtures based on squalane for clarity

are shown in Fig. 8. In its lower part, the relative deviations of the σ values for the binary mixtures from those of the pure solvents are given.

The results from SLS depicted in Fig. 8 show that the data for σ of the binary mixtures based on the solvents HMN, squalane, and *n*-triacontane are mostly within combined uncertainties relative to the values for the pure solvents. This agrees with the investigations of the binary mixtures consisting of He dissolved in *n*-hexadecane [20]. In a similar way as found for η_L , a distinct difference between σ of the binary mixtures and the pure solvents was only visible in the case of 2-butyl-1-octanol with a maximum deviation of about 7% at $p=7.0$ MPa. This difference may be related to a larger density of 2-butyl-1-octanol [34] and denser packing of the molecules in mixtures with dissolved He.

Also the results from EMD simulations shown on the right-hand side of Fig. 8 predict only a small influence of the dissolved He on σ compared to the pure solvents. Here, all results for the mixtures agree within the combined uncertainties with the values for the pure solvents. The maximum deviation can be observed for the mixture of He dissolved in HMN at the highest investigated T and is -4.9% .

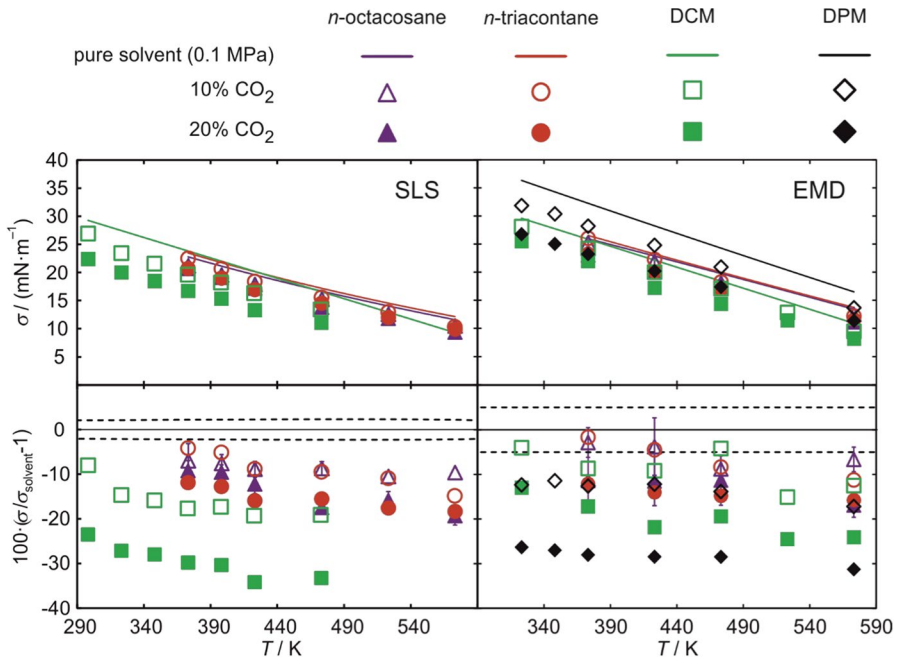


Fig. 9 (Top) Interfacial tension σ of the binary mixtures consisting of CO_2 dissolved in n -octacosane, n -triacontane, or DCM investigated by SLS (left) and EMD simulations (right) as a function of T and CO_2 mole fraction (open and closed symbols). In the case of EMD simulations, also results for binary mixtures based on DPM are shown. For comparison, the correlations for σ of the pure solvents based on data obtained by SLS [17, 34, 39] and EMD simulations [34] are shown (solid line). (Bottom) Relative deviations between the binary mixtures and the pure solvents. The dotted lines mark the average expanded uncertainty ($k=2$) of the properties for the pure solvents. Error bars are shown only exemplarily for the mixtures based on n -octacosane for clarity. The mole fractions of the dissolved gas given in the legend are approximate values. The real composition at each T can be taken from Tables 2 and S4

Considering the weak influence of dissolved He on σ , good agreement between data from SLS and EMD simulations can be observed for the present systems.

Finally, σ of binary mixtures consisting of CO_2 dissolved in the hydrocarbons n -octacosane, n -triacontane, or DCM investigated by SLS and EMD simulations are shown in the upper part of Fig. 9. In the case of EMD simulations, the binary mixtures consisting of DPM with dissolved CO_2 at $x_{\text{CO}_2}=0.1$ or 0.2 were additionally investigated for $T=(323.15$ to $573.15)$ K. For comparison, the T -dependent correlations for σ of the pure solvents determined by SLS [17, 34, 39] and EMD simulations [34] are shown in Fig. 9. Relative deviations of σ of the binary mixtures from the ones of the pure solvents are given in the lower part of Fig. 9.

The results in Fig. 9 from SLS show a clear reduction in σ by adding dissolved CO_2 to the three investigated solvents. For the solvents n -octacosane and n -triacontane, the deviations of the mixture data from the pure solvent data are in the range between $-(5$ and $20)\%$ and generally increase with increasing x_{CO_2} . For these two solvents, the deviation between σ of the mixture and the pure solvent increases with

increasing T . For the binary mixtures based on DCM, the reduction in σ is more pronounced and ranges up to -35% . Also here, the deviations increase with increasing T . The reduction of the interfacial tension by the addition of CO_2 to hydrocarbons can be related to the distinct enrichment of CO_2 at the vapor–liquid interface, as it was observed by EMD simulations in its mixtures with n -hexane [19] and n -hexadecane [20].

The EMD simulations also predict a reduced interfacial tension of the mixtures compared to the pure solvents for all investigated mixtures. This reduction increases with increasing amount of dissolved CO_2 and with increasing σ of the pure solvents. While the magnitude of the reduction found by EMD simulations agrees well with the observations from SLS in the case of the two linear alkanes, it is underestimated by EMD simulations in the case of DCM. At $T=473$ K, for example, EMD simulations predict a reduction of σ for the DCM-based mixture at $x_{\text{CO}_2}=0.2$ of 19%, while the results from SLS show a deviation of 33%. Finally, the comparison between the DCM- and DPM-based mixtures shows a stronger influence of the dissolved CO_2 for the DPM-based mixtures. This can be explained by the larger σ of DPM in comparison with DCM, which seems to cause a stronger enrichment of CO_2 molecules at the vapor–liquid interface and, thus, a stronger decrease in mixtures with DPM.

5 Conclusions

In the present study, results for η_L and σ of the binary mixtures consisting of various linear, branched, cyclic, or oxygenated hydrocarbons with different dissolved gases obtained by SLS experiments and EMD simulations are presented. Binary mixtures of the solvents n -octacosane, n -triacontane, HMN, 2-butyl-1-octanol, squalane, DCM, or DPM with the solutes H_2 , He, CH_4 , H_2O , CO, or CO_2 were investigated in the T range between (298.15 and 573.15) K and solute mole fractions up to about 0.2. With the SLS technique, η_L and σ of the binary mixtures could be accessed with average expanded experimental uncertainties of (2.4 and 2.3)%, respectively. By comparing the thermophysical properties of the binary mixtures with the ones of the pure solvents, the influence of the dissolved gas on η_L and σ could be analyzed. For mixtures based on n -octacosane or 1-hexadecanol, the solutes CO_2 and CH_4 show a reducing impact on both properties with relative deviations up to -20% compared to the values for the pure solvents. In contrast, the solutes H_2 and CO have a much smaller influence, which is reflected by the agreement of the results for the mixtures with those of the pure substances mostly within combined uncertainties. For the solute H_2O , no differences between viscosities and interfacial tensions of the binary mixtures and those of pure n -octacosane were found. For mixtures consisting of H_2O dissolved in 1-hexadecanol, on the other hand, a distinct increase in η_L and σ in comparison to the data for pure 1-hexadecanol was found, which seems to be related to the impact of hydrogen bonding. When comparing the influence of the solutes He and CO_2 , clear differences were found. In general, a reduction in η_L and σ relative to the pure solvent data was found in the case of CO_2 , while the results for mixtures containing He are not distinctly affected and usually agree within combined uncertainties with the data for the solvents. Results from EMD simulations

have shown that the employed FFs for the solvents and solutes are not able to quantitatively predict the influence of the dissolved gases on η_L , and often also not in a qualitative way. In the case of σ , on the other hand, the results calculated from EMD simulation agree much better with the SLS data and the simulations are able to predict the influence of the dissolved gases in most cases.

Supplementary Information The online version contains supplementary material available at <https://doi.org/10.1007/s10765-022-03012-1>.

Acknowledgements This work was financially supported by the German Research Foundation (Deutsche Forschungsgemeinschaft, DFG) via the project Grants FR 1709/15-1. The authors gratefully acknowledge funding of the Erlangen Graduate School in Advanced Optical Technologies (SAOT) by the Bavarian State Ministry for Science and Art and further gratefully acknowledge the computing resources and support provided by the Erlangen Regional Computing Center (RRZE). The authors acknowledge Johannes Knorr for his support in the experimental determination of the viscosity and interfacial tension.

Funding Open Access funding enabled and organized by Projekt DEAL.

Declarations

Conflict of Interest The authors have no competing interests to declare that are relevant to the content of this article.

Open Access This article is licensed under a Creative Commons Attribution 4.0 International License, which permits use, sharing, adaptation, distribution and reproduction in any medium or format, as long as you give appropriate credit to the original author(s) and the source, provide a link to the Creative Commons licence, and indicate if changes were made. The images or other third party material in this article are included in the article's Creative Commons licence, unless indicated otherwise in a credit line to the material. If material is not included in the article's Creative Commons licence and your intended use is not permitted by statutory regulation or exceeds the permitted use, you will need to obtain permission directly from the copyright holder. To view a copy of this licence, visit <http://creativecommons.org/licenses/by/4.0/>.

References


1. S. Lee, A. Sardesai, *Top. Catal.* **32**, 197 (2005). <https://doi.org/10.1007/s11244-005-2891-8>
2. S. Lee, M.R. Gogate, C.J. Kulik, *Chem. Eng. Sci.* **47**, 3769 (1992). [https://doi.org/10.1016/0009-2509\(92\)85096-T](https://doi.org/10.1016/0009-2509(92)85096-T)
3. F.G. Ación Fernández, J.M. Fernández Sevilla, E. Molina Grima, *Rev. Environ. Sci. Biotechnol.* **12**, 131 (2013). <https://doi.org/10.1007/s11157-012-9307-6>
4. S.T. Summerfelt, B.J. Vinci, R.H. Piedrahita, *Aquac. Eng.* **22**, 87 (2000). [https://doi.org/10.1016/S0144-8609\(00\)00034-0](https://doi.org/10.1016/S0144-8609(00)00034-0)
5. D. Langevin, *Light Scattering by Liquid Surfaces and Complementary Techniques* (Marcel Dekker, New York, 1992)
6. E.H. Lucassen-Reynders, J. Lucassen, *Adv. Colloid Interfaces* **2**, 347 (1970). [https://doi.org/10.1016/0001-8686\(70\)80001-X](https://doi.org/10.1016/0001-8686(70)80001-X)
7. A.P. Fröba, A. Leipertz, *Int. J. Thermophys.* **22**, 41 (2001). <https://doi.org/10.1023/A:1006755502597>
8. A.P. Fröba, *Simultane Bestimmung von Viskosität und Oberflächenspannung transparenter Fluide mittels Oberflächenlichtstreuung*. (Friedrich-Alexander-Universität Erlangen-Nürnberg, Doctoral thesis, Erlangen, 2002)
9. A.P. Fröba, A. Leipertz, *J. Chem. Eng. Data* **52**, 1803 (2007). <https://doi.org/10.1021/je7001623>

10. A.P. Fröba, A. Leipertz, *Int. J. Thermophys.* **24**, 1185 (2003). <https://doi.org/10.1023/A:1026152331710>
11. A.P. Fröba, C. Botero, A. Leipertz, *Int. J. Thermophys.* **27**, 1609 (2006). <https://doi.org/10.1007/s10765-006-0122-6>
12. A.P. Fröba, H. Kremer, A. Leipertz, F. Flohr, C. Meurer, *Int. J. Thermophys.* **28**, 449 (2007). <https://doi.org/10.1007/s10765-007-0178-y>
13. A.P. Fröba, P. Wasserscheid, D. Gerhard, H. Kremer, A. Leipertz, *J. Phys. Chem. B* **111**, 12817 (2007). <https://doi.org/10.1021/jp074799d>
14. A.P. Fröba, H. Kremer, A. Leipertz, *J. Phys. Chem. B* **112**, 12420 (2008). <https://doi.org/10.1021/jp804319a>
15. T. Koller, M.H. Rausch, P.S. Schulz, M. Berger, P. Wasserscheid, I.G. Economou, A. Leipertz, A.P. Fröba, *J. Chem. Eng. Data* **57**, 828 (2012). <https://doi.org/10.1021/jc201080c>
16. T.M. Koller, F.D. Lenahan, P.S. Schmidt, T. Klein, J. Mehler, F. Maier, M.H. Rausch, P. Wasserscheid, H.-P. Steinrück, A.P. Fröba, *Int. J. Thermophys.* **41**, 144 (2020). <https://doi.org/10.1007/s10765-020-02720-w>
17. M. Kerscher, T. Klein, P.S. Schulz, E. Veroutis, S. Dürr, P. Preuster, T.M. Koller, M.H. Rausch, I.G. Economou, P. Wasserscheid, A.P. Fröba, *Int. J. Hydrog. Energy* **45**, 28903 (2020). <https://doi.org/10.1016/j.ijhydene.2020.07.261>
18. P.S. Schmidt, M. Kerscher, T. Klein, J.H. Jander, F.E. Berger Bioucas, T. Rüde, S. Li, M. Stadelmaier, S. Hanyon, R.R. Fathalla, A. Bösmann, P. Preuster, P. Wasserscheid, T.M. Koller, M.H. Rausch, A.P. Fröba, *Int. J. Hydrog. Energy* **47**, 6111 (2022). <https://doi.org/10.1016/j.ijhydene.2021.11.198>
19. T.M. Koller, S. Yan, C. Steininger, T. Klein, A.P. Fröba, *Int. J. Thermophys.* **40**, 79 (2019). <https://doi.org/10.1007/s10765-019-2544-y>
20. T. Klein, F.D. Lenahan, M. Kerscher, J.H. Jander, M.H. Rausch, T.M. Koller, A.P. Fröba, *J. Chem. Eng. Data* **66**, 3205 (2021). <https://doi.org/10.1021/acs.jced.1c00289>
21. C. Giraudet, T. Klein, G. Zhao, M.H. Rausch, T.M. Koller, A.P. Fröba, *J. Phys. Chem. B* **122**, 3163 (2018). <https://doi.org/10.1021/acs.jpcc.8b00733>
22. T. Klein, W. Wu, M.H. Rausch, C. Giraudet, T.M. Koller, A.P. Fröba, *J. Phys. Chem. B* **122**, 7122 (2018). <https://doi.org/10.1021/acs.jpcc.8b03568>
23. W. Wu, T. Klein, M. Kerscher, M.H. Rausch, T.M. Koller, C. Giraudet, A.P. Fröba, *J. Phys. Chem. B* **124**, 2482 (2020). <https://doi.org/10.1021/acs.jpcc.0c00646>
24. K.D. Papavasileiou, O.A. Moulτος, I.G. Economou, *Fluid Phase Equilib.* **476**, 30 (2018). <https://doi.org/10.1016/j.fluid.2017.05.004>
25. K.D. Papavasileiou, L.D. Peristeras, A. Bick, I.G. Economou, *J. Phys. Chem. B* **123**, 6229 (2019). <https://doi.org/10.1021/acs.jpcc.9b02840>
26. Y.M. Muñoz-Muñoz, G. Guevara-Carrion, J. Vrabec, *J. Phys. Chem. B* **122**, 8718 (2018). <https://doi.org/10.1021/acs.jpcc.8b05610>
27. W. Wu, T. Klein, M. Kerscher, M.H. Rausch, T.M. Koller, C. Giraudet, A.P. Fröba, *J. Phys. Chem. B* **123**, 8777 (2019). <https://doi.org/10.1021/acs.jpcc.9b06211>
28. S. Becker, S. Werth, M. Horsch, K. Langenbach, H. Hasse, *Fluid Phase Equilib.* **427**, 476 (2016). <https://doi.org/10.1016/j.fluid.2016.08.007>
29. D.C. Rapaport, *The Art of Molecular Dynamics Simulation*, 2nd edn. (Cambridge University Press, Cambridge, 2004)
30. M.P. Allen, D.J. Tildesley, *Computer Simulation of Liquids* (Oxford University Press, New York, 1987)
31. D. Frenkel, B. Smit, *Understanding Molecular Simulation: From Algorithms to Applications* (Academic Press, San Diego, 2002)
32. S.W.I. Siu, K. Pluhackova, R.A. Böckmann, *J. Chem. Theory Comput.* **8**, 1459 (2012). <https://doi.org/10.1021/ct200908r>
33. K. Pluhackova, H. Morhenn, L. Lautner, W. Lohstroh, K.S. Nemkovski, T. Unruh, R.A. Böckmann, *J. Phys. Chem. B* **119**, 15287 (2015). <https://doi.org/10.1021/acs.jpcc.5b08569>
34. T. Klein, F.D. Lenahan, M. Kerscher, M.H. Rausch, I.G. Economou, T.M. Koller, A.P. Fröba, *J. Phys. Chem. B* **124**, 4146 (2020). <https://doi.org/10.1021/acs.jpcc.0c01740>
35. F.D. Lenahan, M. Zikeli, M.H. Rausch, T. Klein, A.P. Fröba, *J. Chem. Eng. Data* **66**, 2264 (2021). <https://doi.org/10.1021/acs.jced.1c00108>
36. J.H. Jander, P.S. Schmidt, C. Giraudet, P. Wasserscheid, M.H. Rausch, A.P. Fröba, *Int. J. Hydrog. Energy* **46**, 19446 (2021). <https://doi.org/10.1016/j.ijhydene.2021.03.093>

37. A.P. Fröba, A. Leipertz, *Int. J. Thermophys.* **24**, 895 (2003). <https://doi.org/10.1023/A:1025097311041>
38. A.P. Fröba, L.P. Pellegrino, A. Leipertz, *Int. J. Thermophys.* **25**, 1323 (2004). <https://doi.org/10.1007/s10765-004-5741-1>
39. T.M. Koller, T. Klein, C. Giraudet, J. Chen, A. Kalantar, G.P. van der Laan, M.H. Rausch, A.P. Fröba, *J. Chem. Eng. Data* **62**, 3319 (2017). <https://doi.org/10.1021/acs.jced.7b00363>
40. T. Klein, J. Cui, A. Kalantar, J. Chen, M.H. Rausch, T.M. Koller, A.P. Fröba, *J. Chem. Eng. Data* **64**, 817 (2019). <https://doi.org/10.1021/acs.jced.8b01139>
41. T. Klein, S. Yan, J. Cui, J.W. Magee, K. Kroenlein, M.H. Rausch, T.M. Koller, A.P. Fröba, *J. Chem. Eng. Data* **64**, 4116 (2019). <https://doi.org/10.1021/acs.jced.9b00525>
42. B. Poling, J.M. Prausnitz, J.P. O'Connell, *The Properties of Gases and Liquids*, 5th edn. (McGraw-Hill, New York, 2001)
43. S. Bo, R. Battino, E. Wilhelm, *J. Chem. Eng. Data* **38**, 611 (1993). <https://doi.org/10.1021/je00012a035>
44. P.J. Hesse, R. Battino, P. Scharlin, E. Wilhelm, *J. Chem. Eng. Data* **41**, 195 (1996). <https://doi.org/10.1021/je9502455>
45. B.B. Breman, A.A.C.M. Beenackers, E.W.J. Rietjens, R.J.H. Stege, *J. Chem. Eng. Data* **39**, 647 (1994). <https://doi.org/10.1021/je00016a004>
46. S.H. Huang, H.M. Lin, K.C. Chao, *J. Chem. Eng. Data* **33**, 143 (1988). <https://doi.org/10.1021/je00052a025>
47. M.J. Abraham, T. Murtola, R. Schulz, S. Páll, J.C. Smith, B. Hess, E. Lindahl, *SoftwareX* **1–2**, 19 (2015). <https://doi.org/10.1016/j.softx.2015.06.001>
48. B. Hess, H. Bekker, H.J.C. Berendsen, J.G.E.M. Fraaije, *J. Comput. Chem.* **18**, 1463 (1997). [https://doi.org/10.1002/\(SICI\)1096-987X\(199709\)18:12%3c1463::AID-JCC4%3e3.0.CO;2-H](https://doi.org/10.1002/(SICI)1096-987X(199709)18:12%3c1463::AID-JCC4%3e3.0.CO;2-H)
49. X.Y. Meng, Y.K. Sun, F.L. Cao, J.T. Wu, V. Vesovic, *J. Phys. Chem. Ref. Data* **47**, 033102 (2018). <https://doi.org/10.1063/1.5039595>
50. E.W. Lemmon, I.H. Bell, M.L. Huber, M.O. McLinden, REFPROP, Standard Reference Data Program. Version 10.0. (National Institute of Standards and Technology, Gaithersburg, MD, 2018)
51. M. Mohammed, F. Ciotta, J.P.M. Trusler, *J. Chem. Eng. Data* **62**, 422 (2017). <https://doi.org/10.1021/acs.jced.6b00750>
52. J. Cui, S. Bi, A.P. Fröba, J. Wu, *J. Chem. Thermodyn.* **152**, 106266 (2021). <https://doi.org/10.1016/j.jct.2020.106266>
53. J. Cui, J. Wu, S. Bi, *Fluid Phase Equilib.* **534**, 112951 (2021). <https://doi.org/10.1016/j.fluid.2021.112951>
54. T. Ono, M. Kyoda, R. Amezawa, M. Ota, Y. Sato, H. Inomata, *Fluid Phase Equilib.* **453**, 13 (2017). <https://doi.org/10.1016/j.fluid.2017.09.005>
55. H.J.C. Berendsen, J.R. Grigera, T.P. Straatsma, *J. Phys. Chem.* **91**, 6269 (1987). <https://doi.org/10.1021/j100308a038>

Publisher's Note Springer Nature remains neutral with regard to jurisdictional claims in published maps and institutional affiliations.

Authors and Affiliations

Tobias Klein¹  · Frances D. Lenahan¹ · Ziwen Zhai¹ · Manuel Kerscher¹ · Julius H. Jander¹ · Thomas M. Koller¹ · Michael H. Rausch¹ · Andreas P. Fröba¹

✉ Tobias Klein
tobias.klein@fau.de

¹ Institute of Advanced Optical Technologies – Thermophysical Properties (AOT-TP), Department of Chemical and Biological Engineering (CBI) and Erlangen Graduate School in Advanced Optical Technologies (SAOT), Friedrich-Alexander-Universität Erlangen-Nürnberg (FAU), Paul-Gordan-Straße 8, 91052 Erlangen, Germany